7
Inertia Coupling and Spin

7.1 Introduction

In the preceding chapters, we have studied the airplane stability, dynamics, and control with the assumption that the longitudinal and lateral-directional motions of the airplane could be decoupled and studied separately. With these assumptions, the problem of airplane dynamics and control was linearized so that the analyses methods of linear systems could be used. For example, the response of the airplane to a 2-deg elevator input would be exactly double that for a 1-deg elevator input. Also, there was no cross coupling between the longitudinal and lateral-directional degrees of freedom. In other words, operating the rudder or the ailerons would not generate any pitching motion or a change in the forward speed or a change in the angle of attack. Similarly, moving the elevator would not generate any sideslip, rolling, or yawing motion. As a consequence, one had to solve the problem for only one set of control inputs and, using those solutions, the response to any other combination of control inputs could be quickly deduced. Furthermore, the response to combined control inputs was the sum of the responses to individual control inputs. In other words, the flight dynamicist had to solve the problem only once. Then, he had it solved for all other cases. What could be simpler?

However, this type of simple approach cannot be used for problems in which the longitudinal and lateral motions are coupled. Such coupling occurs because of either inertial cross coupling or aerodynamic nonlinearities. The examples of the first category are the inertia or roll coupling problems and the spinning motion. We will study these two problems in this chapter. The cross coupling between longitudinal and lateral motions due to aerodynamic nonlinearities and large amplitude motions occurs in flight at high angles of attack close to or exceeding the stalling angle. We will study these problems in Chapter 8.

7.2 Inertia Coupling

The problem of inertia coupling was totally unknown to the aeronautical engineer until the closing years of World War II. During a demonstration flight in late 1944, the German fighter aircraft Heinkel 162 disintegrated in a fast high-speed rolling maneuver. The Heinkel 162 was a small single-engine jet fighter. It so happened that a number of cameras recorded this event, which helped a close reconstruction of the entire episode. However, with the knowledge and expertise available then, no one could come up with a convincing explanation as to why the Heinkel 162 aircraft behaved that way. The second example was that of the British Fairey Delta aircraft during an air show at Farnborough, England. This aircraft had an impressive roll rate capability of 500 deg/s. Halfway through the roll, the pilot lost control, or more appropriately, the airplane took over. Luckily, this incidence did not result in a fatality or severe damage to the aircraft. The

Fairey Delta aircraft carried extensive flight test instrumentation, which recorded the event. Once again, this incident offered a frustrating puzzle because no calculated response even with wild assumptions about the misbehaved aerodynamics could come near the observed motion of the Fairey Delta aircraft. At the same time, the very same approach gave perfectly good results when the roll rate was small.

These two examples demonstrate vividly the essential features of the problem now known as inertia coupling or roll coupling. It has been widely recognized that inertia coupling will occur on aircraft that have long slender fuselages and short aspect ratio wings and have most of their mass concentrated in the fuselage. Such aircraft have a low value of moment of inertia about the longitudinal (x) axis and fairly large values of moments of inertia about y- and z-axes. Furthermore, it is also understood that a loss of either longitudinal (pitch) stability or the directional stability compounds this problem further. This type of mass/inertia distribution and stability characteristics are typical of modern high-speed fighter aircraft.

A fundamental analysis of inertia coupling was presented by Philips in 1948.[1] He examined the stability of a steadily rolling aircraft. He assumed that all the disturbance variables except the steady roll rate were small. He also ignored the damping in pitch and yaw. Based on this analysis, he demonstrated that a steadily rolling airplane deficient in pitch stability experiences a divergence in pitch, whereas one deficient in directional stability experiences a divergence in yaw or sideslip. Even though this simple analysis did not actually consider the real rolling maneuvers like that of the Heinkel 162 or Fairey Delta aircraft, it helped the flight dynamicist identify the root cause of the problem. Since then, the problem of inertia coupling has received considerable attention from many authors who have performed more rigorous analyses of this problem. Interested readers may refer to the literature for more information on this subject.[2–6]

In this section, we will first present a brief physical explanation of the problem of inertia coupling. Then, we will develop the theory of stability of a steadily rolling aircraft and derive Philip's criteria for divergence in pitch or yaw.

7.2.1 Yaw and Pitch Divergence in Rolling Maneuvers

To understand the basic physical principles of inertia coupling, let us assume that the mass of the airplane is concentrated in four distinct lumps at the extremities of the fuselage and wings as shown in Fig. 7.1. The two masses M_1 and M_2 at either end of the fuselage represent the inertia in pitch I_y, and the two masses M_3 and M_4 at the wingtips represent the roll inertia I_x. All the four masses acting together contribute to the inertia in yaw I_z.

Now let us consider what happens when the aircraft starts rolling about its longitudinal (x) axis as shown in Fig. 7.1a. The fuselage masses M_1 and M_2 representing the inertia in pitch do not develop any centrifugal reaction, whereas the wing masses representing the roll inertia develop equal and opposite centrifugal reactions that will try to tear the wings apart. Because they cancel each other, these forces do not cause any inertia coupling but concern the structural engineer who has to provide enough strength and rigidity to the airframe to deal with this situation.

Now let us assume that, for some reason, the rolling aircraft is disturbed in yaw from an equilibrium condition. For this case, all four masses are subjected to centrifugal reactions as shown in Fig. 7.1b. The fuselage masses M_1 and M_2

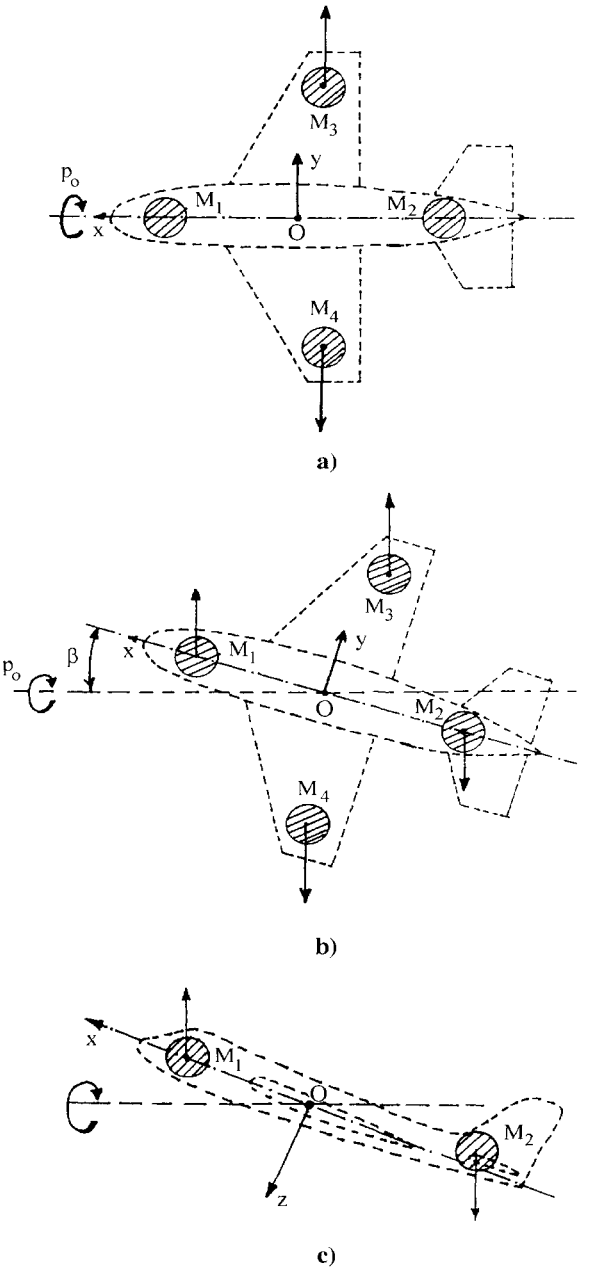

Fig. 7.1 Schematic illustration of inertia coupling effects.

representing the inertia in pitch will attempt to further increase the yaw, and the wing masses M_3 and M_4 representing the inertia in roll will try to reduce yaw and restore the aircraft to its original equilibrium condition. Whether the net result is stabilizing or destabilizing depends on the relative magnitudes of these two centrifugal reactions. If the inertia in pitch exceeds the inertia in roll, which is usually the case for most of the modern combat aircraft, then the destabilizing couple will dominate. Whether the aircraft will experience a divergence in yaw because of this destabilizing inertia-induced yawing couple depends on the level of static directional stability. If the restoring yawing moment due to directional stability overpowers the inertia-induced destabilizing yawing moment, the aircraft returns to its equilibrium condition. If not, the aircraft will experience a divergence in yaw or sideslip. This phenomenon is known as the roll–yaw coupling.

Now let us consider another situation where the aircraft is rolling about the velocity vector as shown in Fig. 7.1c. Such a rolling motion is usually preferred at high angles of attack to avoid the sideslip buildup. In this case, only the fuselage masses representing pitch inertia will contribute to the centrifugal reaction, which produces a destabilizing couple in pitch. If this destabilizing inertia-induced pitching moment is greater than the restoring moment due to static longitudinal stability, the aircraft will experience a divergence in pitch. In other words, an aircraft deficient in static longitudinal stability is prone to divergence in pitch due to inertia coupling during velocity vector rolls.

The pitch inertia increases with the length of the fuselage, thereby increasing the magnitude of the destabilizing inertia-induced pitching couple. Furthermore, to improve performance, modern fighter aircraft compromise static stability in pitch. These two factors make modern combat aircraft vulnerable to inertia cross coupling problems.

7.2.2 Equations of Motion of a Steadily Rolling Aircraft

We have the following force and moment equations [Chapter 4, Eqs. (4.291–4.293, 4.357–4.359)],

$$F_x = m(\dot{U} + qW - rV) \tag{7.1}$$

$$F_y = m(\dot{V} + Ur - pW) \tag{7.2}$$

$$F_z = m(\dot{W} + pV - Uq) \tag{7.3}$$

$$L = \dot{p}I_x - I_{xz}(pq + \dot{r}) + qr(I_z - I_y) \tag{7.4}$$

$$M = \dot{q}I_y + rp(I_x - I_z) + (p^2 - r^2)I_{xz} \tag{7.5}$$

$$N = \dot{r}I_z - I_{xz}(\dot{p} - qr) + pq(I_y - I_x) \tag{7.6}$$

Equations (7.1–7.6) are the complete six-degree-of-freedom equations for the airplane motion. In general, it is difficult to obtain analytical solutions to these equations. In the preceding chapters, we assumed that all the flight-path variables in the disturbed motion are small. With this assumption, we obtained two sets of linear decoupled equations, one set of three equations for longitudinal motion and another set of three equations for lateral-directional motion. Here, for the stability of a steadily rolling airplane, we will proceed along similar lines assuming that all the

disturbance variables are small. Note that the nonzero steady-state roll rate p_0 is not restricted to be small. However, we assume that p_0 is constant so that $\dot{p} = 0$. We need to introduce some more assumptions to simplify the problem further. We will assume that the product of inertia I_{xz} is small so that it can be ignored and further assume that the flight velocity is constant. With the assumptions of constant flight velocity and constant roll rate, Eqs. (7.1) and (7.4) reduce to two algebraic equations. These equations can be used to derive control settings, which is not the main issue here. Hence, we ignore these two equations from our analysis. With these assumptions, we can express the remaining four equations as (see Section 4.3.4)

$$\Delta F_y = mU_0(\Delta\dot{\beta} + r - p_0\Delta\alpha) \tag{7.7}$$

$$\Delta F_z = mU_0(\Delta\dot{\alpha} + p_0\Delta\beta - q) \tag{7.8}$$

$$\Delta M = \dot{q}I_y + rp_0(I_x - I_z) \tag{7.9}$$

$$\Delta N = \dot{r}I_z + p_0q(I_y - I_x) \tag{7.10}$$

Notice that the longitudinal and lateral-directional motions of the aircraft are now coupled because of the nonzero steady-state rolling velocity p_0. However, Eqs. (7.7–7.10) are still linear because we have retained the assumption of small disturbances in all the disturbance variables. For a nonrolling aircraft ($p_0 = 0$), the above equations reduce to two sets of uncoupled, linear equations, one set of two equations for the longitudinal motion (short-period oscillation) and another set of two equations for the lateral-directional motion (Dutch-roll oscillation) as we have studied in Chapter 6.

Divide both sides of Eqs. (7.7) and (7.8) by qS, those of Eq. (7.9) by $qS\bar{c}$ and those of Eq. (7.10) by qSb so that we can express them in the nondimensional form as follows:

$$\Delta C_y = m_1(\Delta\dot{\beta} + r - p_0\Delta\alpha) \tag{7.11}$$

$$\Delta C_z = m_1(\Delta\dot{\alpha} + p_0\Delta\beta - q) \tag{7.12}$$

$$\Delta C_m = \dot{q}I_{y1} + rp_0(I_{x1} - I_{z1}) \tag{7.13}$$

$$\Delta C_n = \dot{r}I'_{z1} + p_0q(I'_{y1} - I'_{x1}) \tag{7.14}$$

where

$$m_1 = \frac{2m}{\rho U_0 S} \tag{7.15}$$

$$I_{x1} = \frac{I_x}{qS\bar{c}} \tag{7.16}$$

$$I_{y1} = \frac{I_y}{qS\bar{c}} \tag{7.17}$$

$$I_{z1} = \frac{I_z}{qS\bar{c}} \tag{7.18}$$

$$I'_{x1} = \frac{I_x}{qSb} \tag{7.19}$$

$$I'_{y1} = \frac{I_y}{qSb} \tag{7.20}$$

$$I'_{z1} = \frac{I_z}{qSb} \tag{7.21}$$

Here, q is the freestream dynamic pressure, S is the wing (reference) area, $\bar{c}$ is the mean aerodynamic chord, and b is the wing span. It may be noted that some of the above nomenclature involving the moments of inertia terms differ from those introduced in Chapter 4.

Let

$$\Delta C_y = C_{y\beta}\Delta\beta \tag{7.22}$$

$$\Delta C_z = C_{z\alpha}\Delta\alpha \tag{7.23}$$

$$\Delta C_m = C_{m\alpha}\Delta\alpha + C_{mq}\left(\frac{q\bar{c}}{2U_0}\right) \tag{7.24}$$

$$\Delta C_n = C_{n\beta}\Delta\beta + C_{nr}\left(\frac{rb}{2U_0}\right) \tag{7.25}$$

For simplicity, we have ignored the acceleration derivatives like $C_{y\dot{\beta}}$, $C_{m\dot{\alpha}}$, and $C_{n\dot{\beta}}$ and other rotary derivatives like C_{yp}, C_{yr}, and C_{np}. With these assumptions, Eqs. (7.22–7.25) can be expressed as follows:

$$m_1 p_0 \Delta\alpha + \left(C_{y\beta} - m_1\frac{\mathrm{d}}{\mathrm{d}t}\right)\Delta\beta - m_1 r = 0 \tag{7.26}$$

$$\left(C_{z\alpha} - m_1\frac{\mathrm{d}}{\mathrm{d}t}\right)\Delta\alpha - m_1 p_0\Delta\beta + m_1 q = 0 \tag{7.27}$$

$$C_{m\alpha}\Delta\alpha + \left(C_{mq}c_1 - I_{y1}\frac{\mathrm{d}}{\mathrm{d}t}\right)q - (I_{x1} - I_{z1})\,p_0 r = 0 \tag{7.28}$$

$$C_{n\beta}\Delta\beta - (I'_{y1} - I'_{x1})p_0 q + \left(C_{nr}b_1 - I'_{z1}\frac{\mathrm{d}}{\mathrm{d}t}\right)r = 0 \tag{7.29}$$

where

$$c_1 = \frac{\bar{c}}{2U_0} \tag{7.30}$$

$$b_1 = \frac{b}{2U_0} \tag{7.31}$$

Taking Laplace transforms, we get

$$m_1 p_0 \Delta\bar{\alpha}(s) + (C_{y\beta} - m_1 s)\Delta\bar{\beta}(s) - m_1\bar{r}(s) = 0 \tag{7.32}$$

$$(C_{z\alpha} - m_1 s)\,\Delta\bar{\alpha}(s) - m_1 p_0 \Delta\bar{\beta}(s) + m_1 \bar{q}(s) = 0 \tag{7.33}$$

$$C_{m\alpha}\Delta\bar{\alpha}(s) + (C_{mq}c_1 - I_{y1}s)\bar{q}(s) - (I_{x1} - I_{z1})p_0\bar{r}(s) = 0 \tag{7.34}$$

$$C_{n\beta}\Delta\bar{\beta}(s) - (I'_{y1} - I'_{x1})p_0\bar{q}(s) + (C_{nr}b_1 - I'_{z1}s)\bar{r}(s) = 0 \tag{7.35}$$

For a nontrivial solution of these equations, we must have

$$\begin{vmatrix} m_1 p_0 & (C_{y\beta} - m_1 s) & 0 & -m_1 \\ (C_{z\alpha} - m_1 s) & -m_1 p_0 & m_1 & 0 \\ C_{m\alpha} & 0 & (C_{mq}c_1 - I_{y1}s) & -(I_{x1} - I_{z1})p_0 \\ 0 & C_{n\beta} & -(I'_{y1} - I'_{x1})p_0 & (C_{nr}b_1 - I'_{z1}s) \end{vmatrix} = 0 \tag{7.36}$$

Expanding the determinant, we get the characteristic equation

$$A_1 s^4 + B_1 s^3 + C_1 s^2 + D_1 s + E_1 = 0 \tag{7.37}$$

where

$$A_1 = m_1^2 I_{y1} I'_{z1} \tag{7.38}$$

$$B_1 = -m_1^2(I_{y1}C_{nr}b_1 + I'_{z1}C_{mq}c_1) - m_1 I_{y1} I'_{z1} C_{z\alpha} - m_1 C_{y\beta} I_{y1} I'_{z1} \tag{7.39}$$

$$\begin{aligned} C_1 = {} & m_1^2 p_0^2 I_{y1} I'_{z1} + C_{y\beta}[m_1(I_{y1}C_{nr}b_1 + I'_{z1}C_{mq}c_1) + I_{y1}I'_{z1}C_{z\alpha}] \\ & - m_1\left[m_1 p_0^2(I_{x1} - I_{z1})(I'_{y1} - I'_{x1}) - C_{z\alpha}(I_{y1}C_{nr}b_1 + I'_{z1}C_{mq}c_1)\right. \\ & \left. - m_1 C_{mq}c_1 C_{nr}b_1 + m_1 C_{m\alpha} I'_{z1}\right] + m_1^2 I_{y1} C_{n\beta} \end{aligned} \tag{7.40}$$

$$\begin{aligned} D_1 = {} & -m_1^2 p_0^2(I_{y1}C_{nr}b_1 + I'_{z1}C_{mq}c_1) + C_{y\beta}\left[-C_{z\alpha}(I_{y1}C_{nr}b_1 + I'_{z1}C_{mq}c_1)\right. \\ & \left. + m_1^2 p_0^2(I_{x1} - I_{z1})(I'_{y1} - I'_{x1}) - m_1 C_{mq}c_1 C_{nr}b_1 + m_1 C_{m\alpha} I'_{z1}\right] \\ & - m_1\left[C_{z\alpha}C_{mq}c_1 C_{nr}b_1 - m_1 C_{m\alpha}C_{nr}b_1 - (I_{x1} - I_{z1})(I'_{y1} - I'_{x1})C_{z\alpha}p_0^2\right] \\ & - m_1 C_{n\beta}(m_1 C_{mq}c_1 + C_{z\alpha}I_{y1}) \end{aligned} \tag{7.41}$$

$$\begin{aligned} E_1 = {} & m_1^2(I_{z1} - I_{x1})(I'_{y1} - I'_{x1})p_0^4 - p_0^2\left[-m_1^2 C_{mq}c_1 C_{nr}b_1 + m_1^2 C_{n\beta}(I_{z1} - I_{x1})\right. \\ & \left. - C_{y\beta}(I_{z1} - I_{x1})(I'_{y1} - I'_{x1})C_{z\alpha} - m_1^2 C_{m\alpha}(I'_{y1} - I'_{x1})\right] \\ & + C_{y\beta}(C_{z\alpha}C_{mq}c_1 C_{nr}b_1 - m_1 C_{m\alpha}C_{nr}b_1) + m_1 C_{n\beta}C_{z\alpha}C_{mq}c_1 - m_1^2 C_{m\alpha}C_{n\beta} \end{aligned} \tag{7.42}$$

Special case, $p_o = 0$. It is interesting to note that in Eqs. (7.38–7.42), wherever the roll rate p_0 appears, it is having only the powers of 2 and 4. For very small values of roll rates $p_0^2 \simeq p_0^4 \simeq 0$. Thus, assuming $p_0 \simeq 0$, Eq. (7.36) reduces to

$$\begin{vmatrix} 0 & (C_{y\beta} - m_1 s) & 0 & -m_1 \\ (C_{z\alpha} - m_1 s) & 0 & m_1 & 0 \\ C_{m\alpha} & 0 & (C_{mq}c_1 - I_{y1}s) & 0 \\ 0 & C_{n\beta} & 0 & (C_{nr}b_1 - I'_{z1}s) \end{vmatrix} = 0 \tag{7.43}$$

Expanding this determinant, we get

$$[-(C_{z\alpha} - m_1 s)(C_{mq} c_1 - I_{y1} s) + m_1 C_{m\alpha}] \times [(C_{y\beta} - m_1 s)(C_{nr} b_1 - I'_{z1} s) + m_1 C_{n\beta}] = 0 \tag{7.44}$$

Expanding the first term, we get

$$s^2 - \left(\frac{C_{z\alpha}}{m_1} + \frac{C_{mq} c_1}{I_{y1}}\right) s + \left(\frac{C_{z\alpha} C_{mq} c_1 - m_1 C_{m\alpha}}{m_1 I_{y1}}\right) = 0 \tag{7.45}$$

Comparing this equation with Eq. (6.51), we recognize that the two equations are identical if we note that we have ignored the damping term $C_{m\dot{\alpha}}$. Thus, the first term in Eq. (7.44) represents the conventional short-period oscillation of the aircraft. Similarly, the second term reduces to

$$s^2 - \left(\frac{m_1 C_{nr} b_1 + C_{y\beta} I'_{z1}}{m_1 I'_{z1}}\right) s + \left(\frac{m_1 C_{n\beta} + C_{y\beta} C_{nr} b_1}{m_1 I'_{z1}}\right) = 0 \tag{7.46}$$

This equation is identical with Eq. (6.219) for the Dutch-roll approximation if we note that we have ignored the C_{yr} term.

Thus, for $p_0 = 0$, the characteristic Eq. (7.37) has a pair of complex roots, one pair for the short-period oscillation and another pair for the Dutch-roll oscillation. We have already studied these two cases in Chapter 6.

Stability criterion for a steadily rolling aircraft. Now, consider the case of a steadily rolling airplane with $p_0 \neq 0$. According to Routh's necessary condition for stability, all the coefficients of the characteristic Eq. (7.37) must be positive or must have the same sign. If any one of the coefficients is negative while at least one other coefficient is positive, the system is likely to become unstable. Normally, the coefficients A_1, B_1, C_1, and D_1 are likely to be positive. The only coefficient that is most likely to become negative is E_1. However, the expression for E_1 as given by Eq. (7.42) is still too complicated to derive a criterion for the stability of a steadily rolling aircraft. Therefore, we need to introduce some more simplifications. As done by Philips,[1] we assume that $C_{mq} = C_{nr} = C_{y\beta} = 0$. With these assumptions, Eq. (7.42) reduces to

$$E_1 = m_1^2 \left[(I_{z1} - I_{x1})(I'_{y1} - I'_{x1}) p_0^4 - p_0^2 (C_{n\beta}(I_{z1} - I_{x1}) - C_{m\alpha}(I'_{y1} - I'_{x1})) - C_{m\alpha} C_{n\beta}\right] \tag{7.47}$$

From Eq. (6.55), we have

$$\omega_\theta = \sqrt{\frac{C_{z\alpha} c_1 C_{mq}}{m_1 I_{y1}} - \frac{C_{m\alpha}}{I_{y1}}} \tag{7.48}$$

Here, ω_θ denotes the natural frequency of the short-period mode. With $C_{mq} = 0$, this equation reduces to

$$\omega_\theta = \sqrt{\frac{-C_{m\alpha}}{I_{y1}}} \tag{7.49}$$

or

$$-C_{m\alpha} = \omega_\theta^2 I_{y1} \tag{7.50}$$

Similarly, using Eq. (6.222) with $C_{nr} = C_{y\beta} = C_{yr} = 0$, we get

$$C_{n\beta} = \omega_\psi^2 I'_{z1} \tag{7.51}$$

Here, ω_ψ denotes the natural frequency of the Dutch-roll mode. Using Eqs. (7.50) and (7.51), Eq. (7.47) can be expressed as

$$E_1 = I_{y1} I'_{z1} m_1^2 \left[\left(\frac{I_{z1} - I_{x1}}{I_{y1}} \right) p_0^2 - \omega_\theta^2 \right] \left[\left(\frac{I'_{y1} - I'_{x1}}{I'_{z1}} \right) p_0^2 - \omega_\psi^2 \right] \tag{7.52}$$

$$= I_{y1} I'_{z1} m_1^2 \left[\left(\frac{I_z - I_x}{I_y} \right) p_0^2 - \omega_\theta^2 \right] \left[\left(\frac{I_y - I_x}{I_z} \right) p_0^2 - \omega_\psi^2 \right] \tag{7.53}$$

Thus, for $E_1 < 0$ (instability), one of the two terms in the square brackets must be negative. Both terms should not become negative at the same time. Thus, we have two conditions for instability. The first condition is given by

$$\left(\frac{I_z - I_x}{I_y} \right) p_0^2 > \omega_\theta^2 \tag{7.54}$$

$$\left(\frac{I_y - I_x}{I_z} \right) p_0^2 < \omega_\psi^2 \tag{7.55}$$

and the second condition is given by

$$\left(\frac{I_z - I_x}{I_y} \right) p_0^2 < \omega_\theta^2 \tag{7.56}$$

$$\left(\frac{I_y - I_x}{I_z} \right) p_0^2 > \omega_\psi^2 \tag{7.57}$$

The first condition is equivalent to

$$\left(\frac{\omega_\theta^2 I_y}{I_z - I_x} \right) < p_0^2 < \left(\frac{\omega_\psi^2 I_z}{I_y - I_x} \right) \tag{7.58}$$

or

$$\left(\frac{\omega_\theta}{p_0} \right)^2 < \left(\frac{I_z - I_x}{I_y} \right) \tag{7.59}$$

and

$$\left(\frac{\omega_\psi}{p_0} \right)^2 > \left(\frac{I_y - I_x}{I_z} \right) \tag{7.60}$$

Suppose we plot $(\omega_\theta / p_0)^2$ vs $(\omega_\psi / p_0)^2$ as shown in Fig. 7.2; then the first condition corresponds to the shaded region I of pitch divergence. Here, the aircraft experiences pitch divergence because it has a smaller level of longitudinal stability

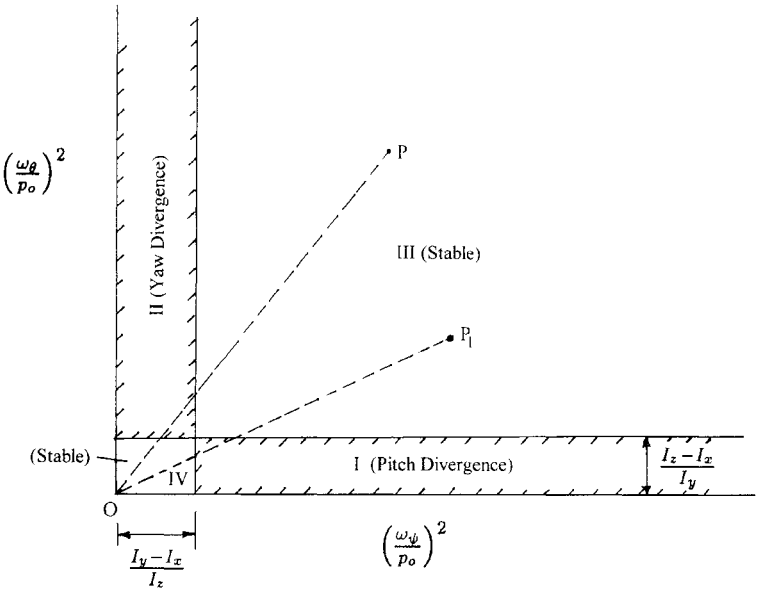

Fig. 7.2 Stability diagram.

as indicated by Eq. (7.59) and a larger level of directional stability as indicated by Eq. (7.60).

Similarly, the second condition given by Eqs. (7.56) and (7.57) can be expressed as

$$\left(\frac{\omega_\psi}{p_0}\right)^2 < \left(\frac{I_y - I_x}{I_z}\right) \tag{7.61}$$

and

$$\left(\frac{\omega_\theta}{p_0}\right)^2 > \left(\frac{I_z - I_x}{I_y}\right) \tag{7.62}$$

which corresponds to the shaded region II of yaw divergence as shown in Fig. 7.2. In this case, the aircraft has a relatively large longitudinal stability as indicated by Eq. (7.62) and a small directional stability as indicated by Eq. (7.61). Thus, if a point lies in region I, then the aircraft experiences a divergence in pitch and, if it lies in region II, it will diverge in yaw or sideslip.

We have two regions, III and IV, where the aircraft is stable. Region III corresponds to those cases where the rolling velocity p_0 is small, and region IV corresponds to large rolling velocities. Let us consider what happens when a given aircraft starts rolling at a steady rate. Initially, let us assume that the roll rate is small so that this condition corresponds to the point P in region III. Note that the slope of the line connecting point P to the origin is equal to the ratio $(\omega_\theta/\omega_\psi)^2$. As the rate of roll increases, we approach the origin along the straight line OP. Because this aircraft has a higher short-period frequency compared to the Dutch-roll

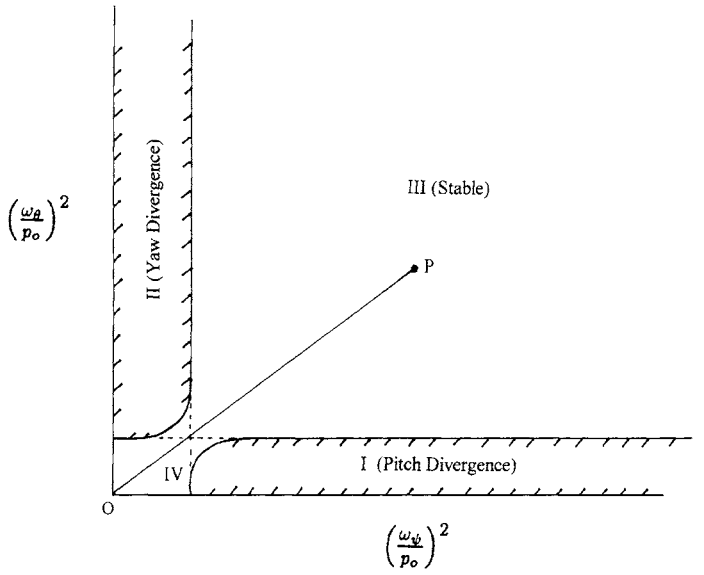

Fig. 7.3 Stability diagram modified because of damping terms.

frequency, at some value of roll rate p_0, the straight line OP will intersect region II, indicating that the aircraft will diverge in yaw or sideslip. On the other hand, if it has a higher Dutch-roll frequency compared to the short-period frequency, it will experience a divergence in pitch as shown by the line OP_1 intersecting region I.

The narrow region around the origin in which the aircraft becomes stable at extremely high roll rates corresponds to the case of spin stabilization. This is the case of artillery shells and bullets, which are known to be flying through the atmosphere at high velocities and at high roll rates without experiencing any inertia coupling problems. Generally, a body becomes spin stabilized about an axis of least inertia. Usually, for modern combat aircraft, the axis of least inertia happens to be the x-body axis about which the aircraft is rolling. So as the roll rate increases, the aircraft becomes spin stabilized.

The stability diagram shown in Fig. 7.2 is sometimes known as Philip's stability diagram.

In the above analysis, for simplicity, we have ignored acceleration and damping derivatives. With the inclusion of these terms, the stability boundaries are modified as shown by the solid lines in Fig. 7.3. Thus, we observe that the narrow region around the origin where the aircraft becomes spin stabilized now connects to the stable region of small rolling velocities. By properly choosing the values of ω_θ and ω_ψ, it is possible to avoid the instabilities in pitch and yaw as shown by the straight line OP. As the roll rate increases, the aircraft simply becomes spin stabilized. However, we must remember that this analysis is based on several simplifying assumptions pertaining to the airplane's mass/inertia distribution and aerodynamic characteristics.

7.2.3 Prevention of Inertia Coupling

For an aircraft prone to divergence in yaw, we can improve its resistance to inertia coupling by increasing the level of static directional stability $C_{n\beta}$ or by increasing the inertia in roll I_x relative to the inertia in pitch I_y. Note that the width of the region II shrinks as we increase I_x relative to I_y. These methods call for major modifications and have to be considered early in the design cycle. As we know, the vertical tail is the major contributor to the static directional stability parameter $C_{n\beta}$. Therefore, to increase $C_{n\beta}$, we have to increase the vertical tail area and vertical tail arm. However, this may cause some problems in spiral stability. Thus, a tradeoff is involved in deciding how much directional stability can be permitted on a given aircraft. The second option calls for distributing more mass into the wings such as placing fuel tanks in the wings. Also, we can have a larger wing span or a higher aspect ratio. This explains why the earlier aircraft that had a short bulky fuselage and high aspect ratio wings did not experience inertia coupling problems.

Similarly, for an aircraft prone to pitch divergence, we can increase its resistance to inertia coupling by increasing the static longitudinal stability level $C_{m\alpha}$ or increasing the inertia in roll I_x relative to the inertia in yaw I_z. The main factors affecting the longitudinal stability parameter $C_{m\alpha}$ are the horizontal tail area, horizontal tail moment arm, and the location of the center of gravity. The designer has to make a proper selection of these variables. However, the second option is of very limited value in this case because we cannot increase I_x without increasing I_z.

Another option is to use a feedback control system, which will increase both the damping in pitch and damping in yaw. Referring to Fig. 7.3, we observe that this will result in widening the area, which connects regions III and IV. However, we will not be going into the design of such a feedback control system. The interested reader may refer elsewhere[7] for additional information on this subject.

Example 7.1

To illustrate the above theory, we consider the following aircraft.[6] The data given in Ref. 6 is in the FPS (foot-pound-second) system, which was converted to SI units as given in the following: mass $= 1.0872 \times 10^4$ kg, $I_x = 1.4881 \times 10^4$ kgm^2, $I_y = 7.7417 \times 10^4$ kgm^2, $I_z = 8.7850 \times 10^4$ kgm^2, wing area $S = 35.0233$ m^2, mean aerodynamic chord $\bar{c} = 3.442$ m, wing span $b = 11.1557$ m, $C_{nr} = -0.095$, $C_{mq} = -3.5$, $C_{m\alpha} = -0.36$, $C_{n\beta} = 0.057$, $C_{y\beta} = -0.28$, $C_{L\alpha} = 3.85$, and $C_{lp} = -0.255$. All the derivatives are per radian.

For flight at a velocity of 210.6168 m/s and a dynamic pressure of 9432.4 N/m^2, examine the stability of this aircraft in steady rolling maneuvers.

Solution. We have

$$\left(\frac{I_z - I_x}{I_y}\right) = \frac{8.7850 \times 10^4 - 1.4881 \times 10^4}{7.7417 \times 10^4}$$

$$= 0.9425$$

$$\left(\frac{I_y - I_x}{I_z}\right) = \frac{7.7417 \times 10^4 - 1.4881 \times 10^4}{8.7850 \times 10^4}$$

$$= 0.7118$$

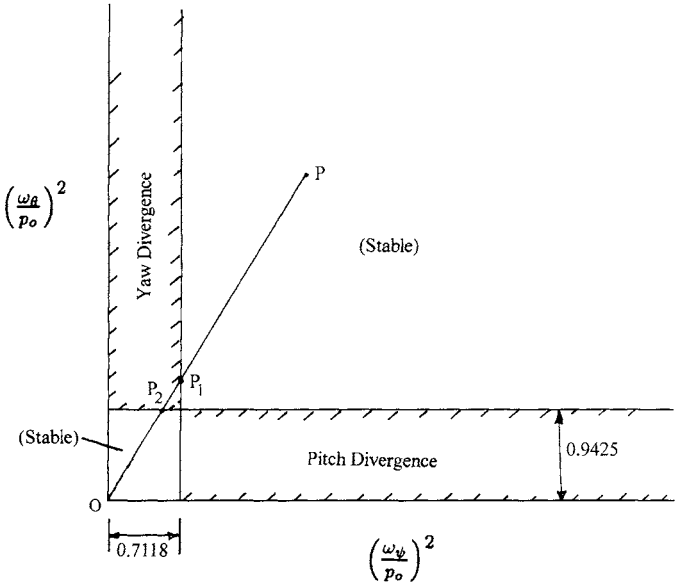

Fig. 7.4 Stability diagram for Example 7.1.

The pitch divergence and yaw divergence boundaries are shown in Fig. 7.4. We have

$$I_{y1} = \frac{I_y}{q S \bar{c}}$$

$$= \frac{7.7417 \times 10^4}{9432.4 \times 35.0233 \times 3.442}$$

$$= 0.06808$$

$$\omega_\theta = \sqrt{\frac{-C_{m\alpha}}{I_{y1}}}$$

$$= \sqrt{\frac{0.36}{0.06808}}$$

$$= 2.299 \text{ rad/s}$$

$$I'_{z1} = \frac{I_z}{q S b}$$

$$= \frac{8.7850 \times 10^4}{9432.4 \times 35.0233 \times 11.1557}$$

$$= 0.0238$$

$$\omega_\psi = \sqrt{\frac{C_{n\beta}}{I'_{z1}}}$$

$$= \sqrt{\frac{0.057}{0.0238}}$$

$$= 1.5476 \text{ rad/s}$$

The slope of the line OP for the given aircraft is given by

$$\left(\frac{\omega_\theta}{\omega_\psi}\right)^2 = 2.2068$$

As the roll rate increases, we move towards the origin along the line OP. When the roll rate increases to that corresponding to point P_1, the aircraft experiences yaw divergence. However, when the roll rate is further increased to that corresponding to P_2, the aircraft becomes stable again (spin stabilized). The roll rates corresponding to P_1 and P_2 are, respectively, equal to 1.8344 and 2.3680 rad/s. Thus, the aircraft experiences yaw divergence due to inertial coupling when

$$1.8344 \text{ rad/s} < p_0 < 2.3680 \text{ rad/s}$$

7.3 Autorotation of Wings and Fuselages

Autorotation is an inherent tendency of unswept wings at angles of attack beyond the stalling angle and is one of the principal causes for a straight-wing, propeller-driven light airplane to enter into a spin. The autorotative tendency of the fuselage also contributes to the development of the spin. However, the autorotative tendencies of the wings and fuselages by themselves are not sufficient to make an airplane develop a steady-state spin. Whether or not an airplane develops a steady-state spin depends on the balance between the aerodynamic and inertial moments as we will discuss later in this chapter.

7.3.1 Autorotation of Wings

Based on strip theory, we have the following expression for damping-in-roll derivative C_{lp} [see Chapter 4, Eq. (4.575)] for a rectangular (unswept) wing of high aspect ratio:

$$(C_{lp})_W = -\tfrac{1}{6}(a_0 + C_D) \tag{7.63}$$

where a_0 is the sectional lift-curve slope and C_D is the sectional drag coefficient. For flight at low angles of attack, a_0 is positive so that $C_{lp} < 0$. For angles of attack above stall, $a_0 < 0$ and, if $|a_0| > C_D$, then the damping-in-roll derivative changes sign and becomes positive ($C_{lp} > 0$). When this happens, the wing becomes unstable in roll. Thus, for instability in roll,

$$a_0 + C_D < 0 \tag{7.64}$$

Equation (7.63) is based on the assumption that the angle of attack is small and is in the linear range. This approximation is satisfactory for most of the airfoils

whose stalling angles are in the range of 10–15 deg. However, if the stalling angles are higher, then the criterion for instability in roll is given by[8]

$$\frac{\partial C_R}{\partial \alpha} < 0 \tag{7.65}$$

where C_R is the resultant force coefficient given by

$$C_R = \sqrt{C_L^2 + C_D^2} \tag{7.66}$$

At high angles of attack exceeding the stalling angle, the resultant force is approximately normal to the chordline so that

$$C_L = C_R \cos\alpha \tag{7.67}$$

$$C_D = C_R \sin\alpha \tag{7.68}$$

Suppose we mount an unswept (rectangular) wing on a single-degree-of-freedom, free-to-roll apparatus having frictionless bearings and place it in the test section of a low-speed wind tunnel at an angle of attack below stall. When it is disturbed from its equilibrium position, the disturbance in roll will quickly die out because $C_{lp} < 0$, and the wing will immediately return to its equilibrium position. However, if the angle of attack is above the stalling angle, the disturbance in roll will increase because $C_{lp} > 0$. In other words, the wing is unstable in roll and starts autorotating. The rate of roll will increase initially but eventually reach a steady value. The steady-state roll rate is called the autorotational speed.

The autorotational characteristics of a wing depend on the nature of the variation of lift and drag coefficients with an angle of attack beyond stall. In Fig. 7.5,

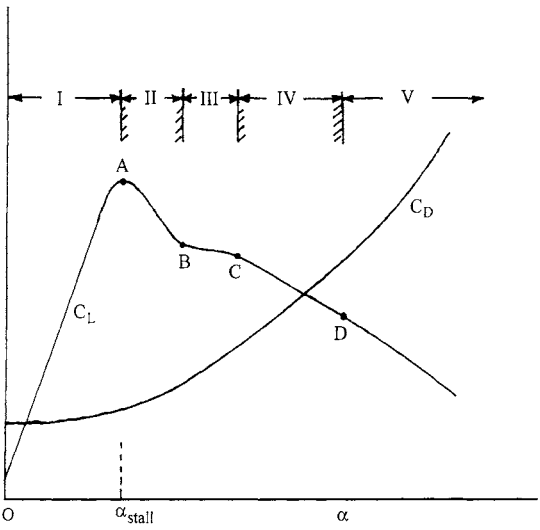

Fig. 7.5 Schematic variations of airfoil lift and drag coefficients with angle of attack.

schematic variations of lift and drag coefficients of an airfoil with angle of attack are shown. Generally, it is possible to identify five regions. In region I, where $\alpha < \alpha_{\text{stall}}$, the damping in roll derivative C_{lp} is negative, and the airfoil is stable in roll. Region II, with $C_{lp} > 0$, is one of spontaneous autorotation because even a slight disturbance will initiate autorotation. In region III, even though the lift-curve slope is negative, the airfoil is stable again because the magnitude of the lift-curve slope is smaller than the drag coefficient. In other words, the damping effect due to drag is sufficient to make the airfoil stable in roll. In region IV, once again the airfoil exhibits autorotative tendency but only to large disturbances in roll so that the angle of attack of the down-going wing falls in region IV and that of the up-going wing in region II. To distinguish this autorotational tendency from the spontaneous autorotative tendency of region II, region IV is called one of latent autorotation. In region V, the airfoil is stable again because of large values of drag coefficient.

7.3.2 Autorotation of Fuselages

The autorotation of a fuselage depends on its cross-sectional shape. Generally, fuselages with circular cross sections or cross sections with round bottoms are resistant to autorotation. On the other hand, cross sections with flat bottoms are prone to autorotation.

To understand the aerodynamics associated with the autorotation of the fuselage, consider a noncircular cylindrical model mounted on a single-degree-of-freedom, free-to-roll apparatus and held at an angle of attack in an airstream of uniform velocity U_0 as shown in Fig. 7.6. We assume that the model is pivoted at its center of gravity and is constrained to rotate about the velocity vector U_0. Let the origin of the body-fixed coordinate system coincide with the center of gravity.

Suppose that the model is imparted a disturbance that makes it rotate in a clockwise direction (viewed from aft end) with an angular velocity Ω. The crossflow angle ϕ at an axial location x (station AA or BB) is given by

$$\phi = \tan^{-1}\left(\frac{\Omega x}{U_0}\right) \tag{7.69}$$

We note that, for the cross sections ahead of the center of gravity, the crossflow angle is positive and, for the sections aft of the center of gravity, the crossflow angle is negative.

The local dynamic pressure at the axial location x is given by

$$q_l = \frac{1}{2}\rho U_0^2\left[1 + \left(\frac{\Omega x \sin\alpha}{U_0}\right)^2\right] \tag{7.70}$$

For simplicity, we assume that the side force coefficient C_y of the fuselage cross sections depends only on the crossflow angle ϕ.

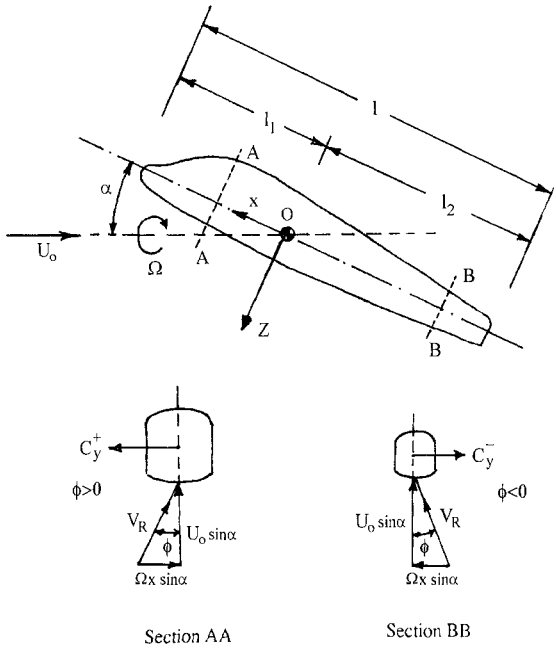

Fig. 7.6 Schematic diagram of an autorotating fuselage.

The moment developed by the section AA about the axis of rotation (velocity vector) is given by

$$\Delta N_\Omega = \frac{1}{2}\rho U_0^2 \left[1 + \left(\frac{\Omega x \sin\alpha}{U_0}\right)^2\right] C_y(\phi) b_0 x \sin\alpha \, dx \tag{7.71}$$

or, in coefficient form,

$$\Delta C_\Omega = \frac{1}{l^2}\left[1 + \left(\frac{\Omega x \sin\alpha}{U_0}\right)^2\right] C_y(\phi) x \sin\alpha \, dx \tag{7.72}$$

where

$$\Delta C_\Omega = \frac{\Delta N_\Omega}{\frac{1}{2}\rho U_0^2 b_0 l^2} \tag{7.73}$$

Here, b_0 is the width of the body, l is the total length of the body, and $x \sin\alpha$ is the moment arm.

Given the variation of C_y with crossflow angle ϕ, an integration of Eq. (7.72) gives the variation of the moment coefficient C_Ω as a function of the angular velocity Ω. The schematic variation of C_Ω is shown in Fig. 7.7. It is possible that this variation is of two types. For type I variation, the yawing moment coefficient

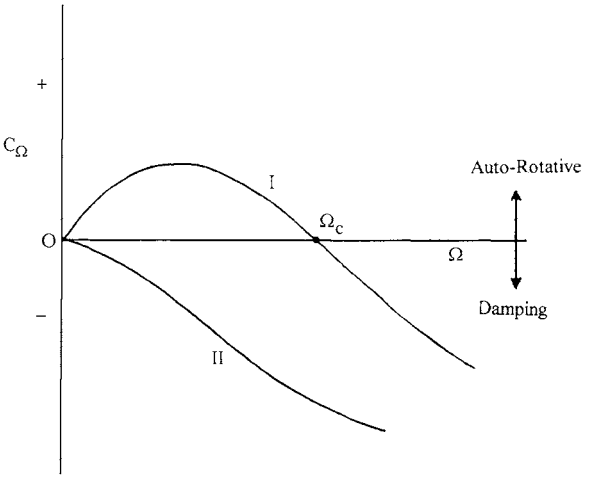

Fig. 7.7 Schematic variation of yawing moment coefficient of a rotating fuselage.

is initially positive and at some point crosses zero and becomes negative for higher values of the angular velocity Ω. Let $\Omega = \Omega_c$ when $C_\Omega = 0$. We observe that for $0 < \Omega < \Omega_c$, $C_\Omega > 0$, which implies that the induced yawing moment will assist the imparted disturbance, and, for $\Omega > \Omega_c$, $C_\Omega < 0$, the induced yawing moment will oppose the rotation. Hence, the angular velocity Ω_c when $C_\Omega = 0$ is the steady-state or equilibrium autorotational speed. If the variation of C_Ω curve is of type II, then the body does not autorotate. It is resistant to autorotation.

The side force variations that can give type I and type II variations of the yawing moment are shown in Fig. 7.8. The type A variation of side force has a positive value of side force for low values of the crossflow angle, and the side force becomes negative for higher values of the crossflow angle. This type of side force variation generates autorotative (yawing) moments on sections close to the center of gravity and damping (yawing) moments for sections away from the center of gravity. Equilibrium or steady autorotation speed is reached when the autorotative moments balance the damping moments so that the net yawing moment on the body is zero. For type B, the side force coefficient is always negative, leading to damping (yawing) moments at all cross sections. This corresponds to type II variation of C_Ω vs Ω as shown in Fig. 7.7.

The cross-sectional shapes having rounded bottom surfaces (Fig. 7.9) generally have type B side force coefficient variation, and those having flat bottom surfaces have type A side force coefficient variation. Rounding the top surface while the bottom surface is kept flat enhances the autorotational tendency.

The Reynolds number is known to have a significant influence on the side force characteristics of noncircular cylinders.[9] For certain cross-sectional shapes, the side force variation changes from type A to type B as the Reynolds number is increased. Thus, it is quite possible that a spin-tunnel model may indicate that the configuration is prospin, whereas full-scale airplane may exhibit an antispin behavior.

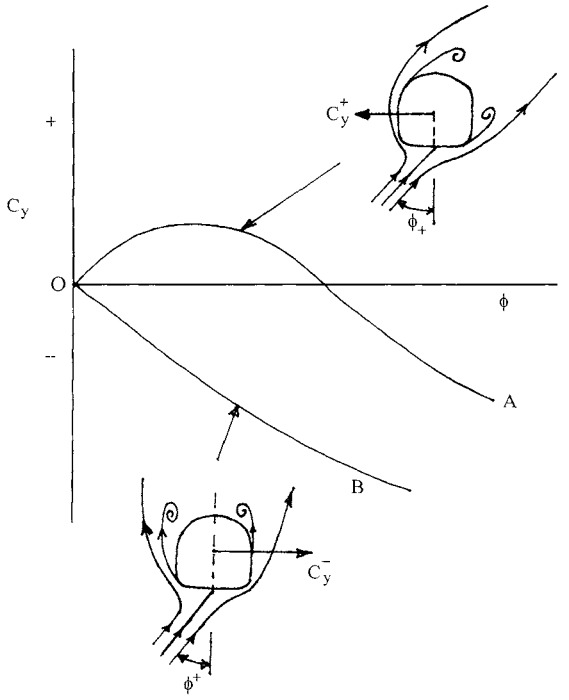

Fig. 7.8 Schematic variation of side force variation in crossflow.

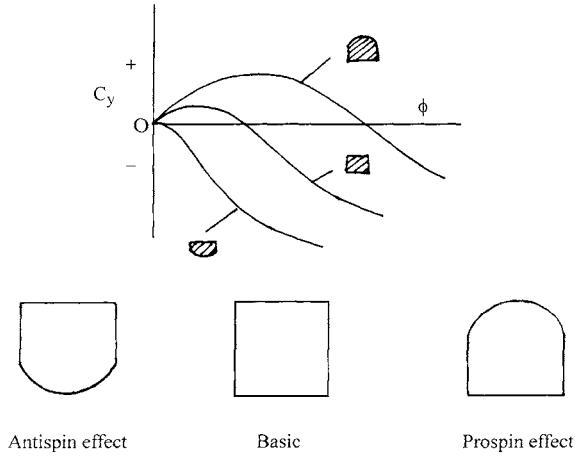

Fig. 7.9 Effect of fuselage cross-sectional shape on spin behavior.

7.4 Airplane Spin

Stall/spin problems have been encountered since the very beginning of aviation. The very low altitudes at which early aircraft were flown precluded the progression of stall to a fully developed spin prior to the ground impact. As a result, it was not possible to clearly ascertain the true causes of these early crashes.

The stall–spin is one of the major causes of light airplane accidents even today. Such an accident is characterized by an inadvertent stall and a spin entry at an altitude that is too low to effect a successful recovery.[10,11] There are three approaches to preventing an inadvertent stall departure:[12] 1) pilot training, 2) stall warning, and 3) increased spin resistance. Although FAA (Federal Aviation Administration) places significant importance on pilot training, the demonstration of competency in spin recovery does not form a part of the private or commercial pilot licensing in the United States. Stall warning systems have helped improve the safety of light general aviation airplanes, but the pilot is still required to take some form of corrective action to prevent the airplane from becoming uncontrollable. Improving the inherent spin resistance offers great potential to make the configuration spinproof and improve the safety of general aviation airplanes.

The straight-wing, light propeller-driven airplanes usually have good longitudinal (pitch) and directional (yaw) stability at stall. The critical aerodynamic characteristic of such airplanes at stall is the autorotative tendency. Also, such airplanes experience an asymmetric stall. In other words, both wings do not stall at the same time, or one wing stalls earlier than the other. One of the possible causes for an asymmetric stall is the propeller sidewash effect. Following an asymmetric stall, the nose drops and the airplane rolls in the direction of the fallen wing and continues to roll owing to the autorotative tendency of the stalled wings. In this process, yawing motion develops due to the aerodynamic roll–yaw coupling. (Note that we are not talking of the inertial roll–yaw coupling here.) Such a motion of the stalled airplane involving combined pitch, roll, and yaw is often called poststall gyration. As the yaw rate builds up, the nose rises, the flight path steepens, and the aircraft starts losing height. The airplane is now in a spin. In spin, the airplane descends vertically downward in a helical path as schematically shown in Fig. 7.10. If a steady-state spin develops, the descent velocity, pitch, roll, and yaw rates attain constant values.

The radius of the helix or the spin radius is usually of the order of one-half of the wing span. However, as the spin becomes flatter, the spin radius decreases further and, in the limiting case, the spin axis may pass through the airplane center of gravity.

Whether or not an airplane develops a steady-state spin depends on the balance between the inertia couples and the aerodynamic moments. If such a balance cannot be achieved, the spinning motion remains oscillatory. Sometimes, this type of spin is also called incipient spin.

In contrast to a straight-wing light airplane, modern aircraft with highly swept wings and long, slender fuselages experience loss of longitudinal and directional stabilities as well as directional control at stall. As a result, the motion following a stall is predominantly in yaw involving directional instability and divergence that may lead to a spin entry.

The spin is not of any tactical value for a military aircraft. Also, it serves no useful purpose in civil aviation. The spin is different from a spiral dive. What distinguishes a spin from the spiral dive is the low air speed and operation of the

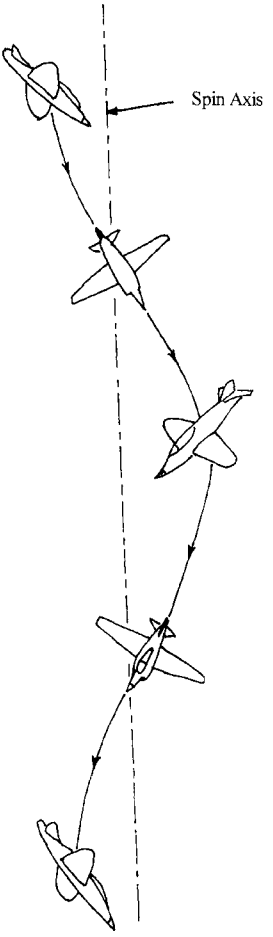

Fig. 7.10 Schematic diagram of a spinning airplane.

wings well beyond the stalling angle. In a spiral dive, the airplane is not stalled and the air speed is continuously increasing. Further, the spin axis is much closer to the airplane center of gravity than the axis of the spiral dive. The airplane has a much higher yaw rate in a spin compared to that in a spiral dive. Typical yaw rates for straight-wing light general aviation airplanes are about 120–150 deg/s in a developed spin.

The spin may be in either direction, i.e., to the right or to the left. However, both the right and left spins may not be identical because of the effect of rotating engine masses or the propellers. The spin may be due to an inadvertent stall or could be intentionally initiated by stalling the airplane and applying prospin controls. Initially, the pitch, roll, and yaw rates oscillate, but these oscillations decay if the airplane establishes a steady spin, in which case all the parameters tend to assume constant values.

The spin may be erect or inverted. In erect spin, the roll (as seen visually by the pilot) and yaw (as indicated by the turn indicator needle) are in the same direction. In an inverted spin, the two are in opposite directions.

The characteristics of the steady-state spin differ between the types of airplanes. No two airplanes spin in the same way. Even airplanes of the same type may spin differently. Also, the spin is affected to a considerable degree by the amount of control deflections used to initiate a spin entry.

Basically, there are two types of erect spins. The first is the steep spin in which the angle of attack is around 30 deg so that the nose is approximately 60 deg below the horizontal plane. The other is the flat spin in which the angle of attack is 60 deg or more. The attitudes of the airplane in steep and flat spins are shown in Fig. 7.11. The steep spin is the slower of the two. In flat spin, the rate of rotation is considerably

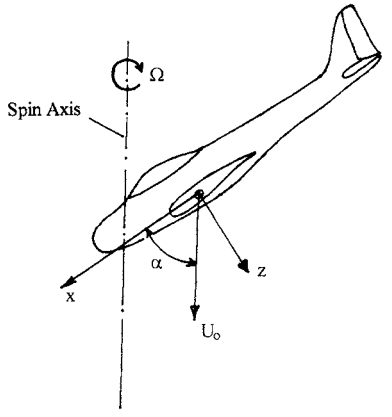

a) Steep spin

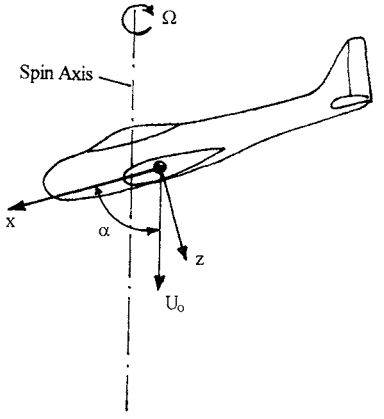

b) Flat spin

Fig. 7.11 Airplane attitudes in spin.

higher. The recovery from the steep spin is relatively easier, whereas recovery from a flat spin may be quite difficult. Usually, a steep spin preceeds a flat spin.

The airplane spin is not very amenable for theoretical analysis because of nonlinear, inertial cross coupling between the longitudinal and lateral degrees of freedom. Furthermore, the aerodynamics of the spinning airplane are extremely complex because of extensive flow separation over the wing and tail surfaces. Owing to these difficulties, most of the investigations of airplane spin have been traditionally based on experimental studies using static and dynamic testing in wind tunnels, rotary balance tests, flying model tests in vertical spin tunnels, outdoor radio-controlled model tests, and full-scale airplane flight tests.[11] Even with this kind of experimental aerodynamic database, it is not always possible to obtain a good correlation between the observed and the predicted spin behavior.

However, if we restrict ourselves to the study of the developed or steady-state spin, it is possible to get some physical understanding of various factors that influence the spinning motion and use the semiempirical approach based on strip theory to get approximate estimates of the aerodynamic coefficients of a steadily spinning airplane.[13–15] In a steady-state spin, the balance of forces is necessary, but this fact alone does not guarantee that the steady-state spin will be established. It is the balance between the inertial and aerodynamic moments that is of crucial importance to the establishment of a steady-state spin. Even for the case of steady-state spin, it is not easy to analytically determine the equilibrium spin modes because 1) a simple and comprehensive analytical aerodynamic model of the spinning airplane is not available and 2) the equations of motion are coupled and nonlinear. An example of determining the steady-state spin modes using the static and dynamic wind-tunnel test data may be found elsewhere.[16]

In this chapter, we will discuss various factors that influence the balance between inertia and aerodynamic moments and also discuss various methods of spin recovery. Finally, we will discuss some of the recent methods for improving the spin resistance of airplanes.

7.5 Equations of Motion for Steady-State Spin

The equations governing the spinning motion are the complete six-degree-of-freedom equations [Eqs. (7.1–7.6)]. For simplicity, we ignore the product of inertia term I_{xz}. With this assumption, Eqs. (7.1–7.6) assume the following form:

$$F_x = m(\dot{U} + qW - rV) \tag{7.74}$$

$$F_y = m(\dot{V} + Ur - pW) \tag{7.75}$$

$$F_z = m(\dot{W} + pV - Uq) \tag{7.76}$$

$$L = \dot{p}I_x + qr(I_z - I_y) \tag{7.77}$$

$$M = \dot{q}I_y + rp(I_x - I_z) \tag{7.78}$$

$$N = \dot{r}I_z + pq(I_y - I_x) \tag{7.79}$$

In a steady-state spin, the spin axis is nearly vertical, and the center of gravity of the airplane moves downward in a helical path around the spin axis with a constant velocity. Let U_0 denote the velocity of descent. Resolving the velocity vector U_0

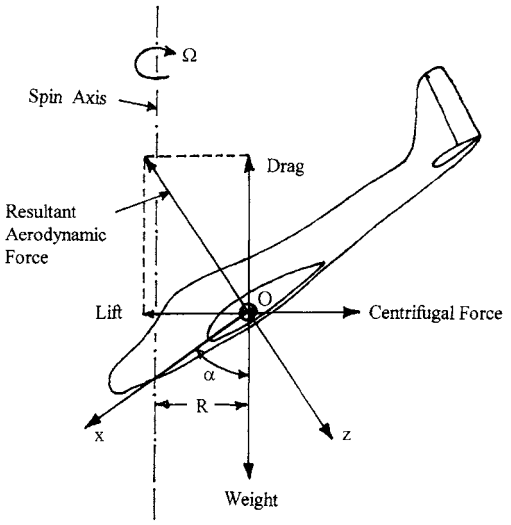

Fig. 7.12 Forces acting on an airplane in steady-state spin.

in the body axes system, we have

$$U = U_0 \cos\alpha \tag{7.80}$$

$$W = U_0 \sin\alpha \tag{7.81}$$

where α is the angle of attack. Because the descent velocity is in a vertical direction, α is the angle between the chordline and the vertical as shown in Fig. 7.12. Note that the spin axis is also vertical.

In a steady-state spin, when viewed from the top, the airplane's center of gravity appears to be moving in a circular path with a constant angular velocity. Let Ω denote this constant angular velocity. Let us assume that the airplane is spinning to its right, i.e., it is rotating in a clockwise direction when viewed from the top. Because of this angular velocity, the airplane will have a component of velocity along the y-body axis. At the center of gravity, the velocity component along the y-body axis is given by

$$V = -\Omega R \tag{7.82}$$

where R is the radius of the helix or the spin radius. As said earlier, the spin radius is usually about one-half of the wing span for steep spins and still smaller for flat spins.

Because in a steady-state spin U, V, and W are constants

$$\dot{U} = \dot{V} = \dot{W} = 0 \tag{7.83}$$

In spin, the angle of attack is well above the stalling angle. At such angles of attack, the resultant aerodynamic force is approximately normal to the wing chordline. Note that the lift acts in the horizontal plane and drag is directed in the vertical plane opposite to the gravity as shown in Fig. 7.12.

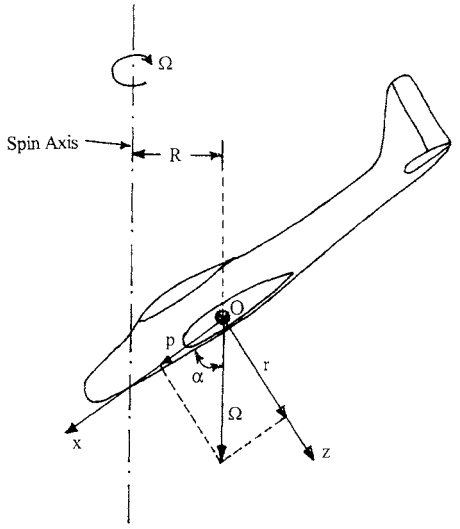

Fig. 7.13 Angular velocity components in spin.

The angular velocity vector Ω can be resolved along the x- and z-body axes (see Fig. 7.13) as

$$p = \Omega \cos\alpha \tag{7.84}$$

$$r = \Omega \sin\alpha \tag{7.85}$$

If the wings are in the horizontal plane,

$$q = 0 \tag{7.86}$$

Because of the helical motion, the spinning airplane experiences a sideslip. For example, in a positive spin (spin to the right), the sideslip is towards the left or port wing, which is also the leading wing. In right spin, the right or starboard wing is the trailing wing. As shown in Fig. 7.14, the sideslip angle is related to the helix angle by the following relation:

$$\beta = -\gamma \tag{7.87}$$

where the helix angle γ is given by

$$\gamma = \tan^{-1}\left(\frac{\Omega R}{U_0}\right) \tag{7.88}$$

Now consider a more general case where the wings are tilted out of the horizontal plane. Let θ_y denote the wing tilt. We assume that θ_y is positive when the right wing is tilted down and the left wing is raised with respect to the horizontal plane as shown in Fig. 7.15. The sideslip is now given by

$$\beta = \theta_y - \gamma \tag{7.89}$$

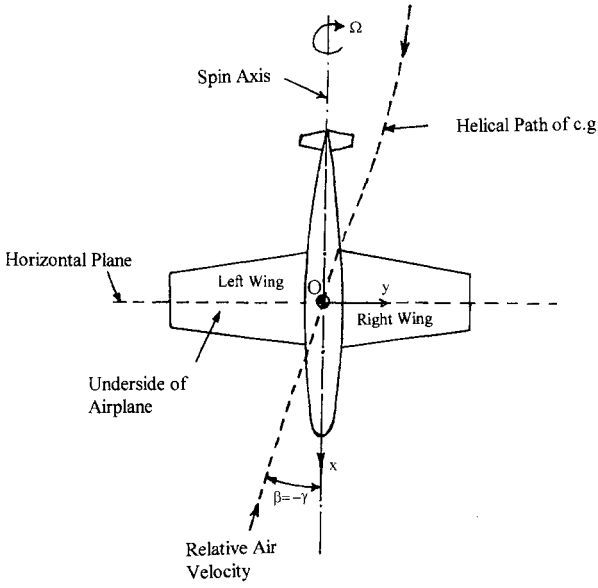

Fig. 7.14 Schematic illustration of sideslip in spin.

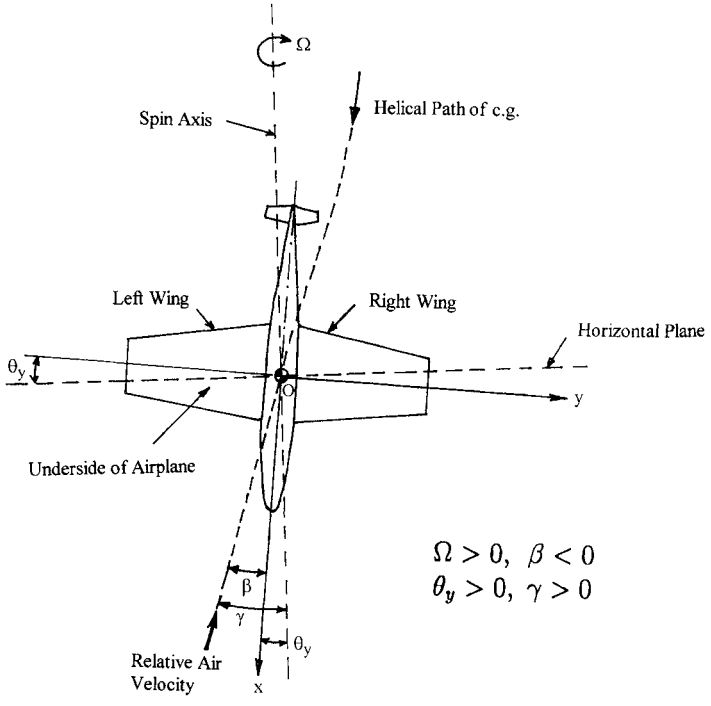

Fig. 7.15 Schematic illustration of the effect of wing tilt in spin.

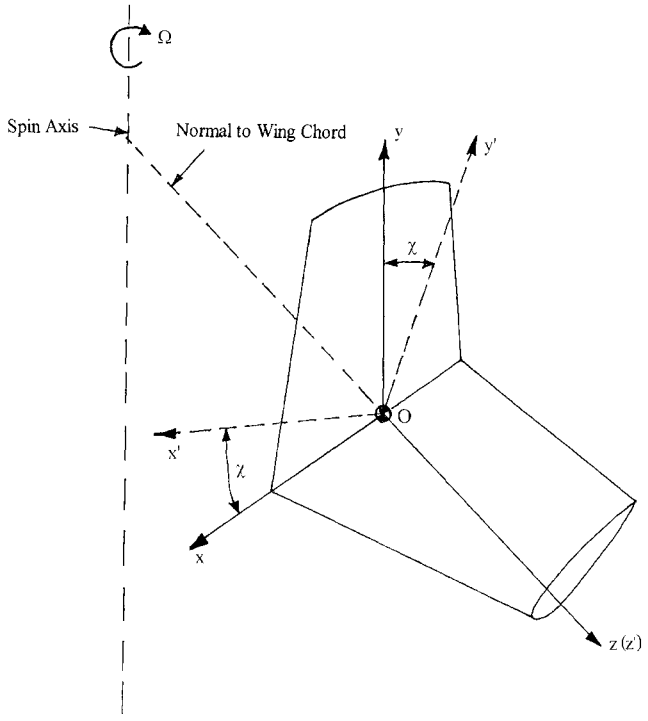

Fig. 7.16 Schematic illustration of rotation about normal-to-wing chord.

We observe that a positive wing tilt θ_y reduces the sideslip. When $\theta_y = \gamma$, the sideslip is zero.

The sideslip plays an important role in the balance of moments. Usually, a certain amount of sideslip is always necessary to achieve a balance of all three components of the moment. Because the centrifugal force acting on all the components of the airplane is directed radially outward and passes through the spin axis, it cannot generate any moment about the spin axis. Therefore, the resultant aerodynamic force must also pass through the spin axis as indicated in Fig. 7.12. Therefore, the only way in which an airplane can have the right amount of wing tilt to adjust the sideslip to the required value is through a rotation about the normal to the chordline as shown in Fig. 7.16. Note that the normal to the wing chordline is along the negative z-body axis. Hence, the airplane essentially rotates about its z-body axis to generate the required amount of wing tilt. Let χ denote the angle by which the aircraft is rotated about the z-body axis. Then the angles χ, θ_y, and α are related by the following expression:[17]

$$\sin\theta_y = -\cos\alpha \sin\chi \tag{7.90}$$

To get a physical understanding of this relation, consider the two extreme cases of $\alpha = 0$ and $\alpha = 90$ deg. At $\alpha = 0$, the spinning motion is all rolling because the x-body axis coincides with the vertical spin axis. The z-body axis is now in the horizontal plane. So the rotation χ about the z-body axis is numerically equal to θ_y.

For $\alpha = 90$ deg, the airplane is in a flat spin, and the spinning motion is all yaw about the z-body axis, which now coincides with the spin axis. Thus, any amount of rotation about the z-body axis does not give any wing tilt because the wings are in the horizontal plane for all values of χ. Hence, the $\theta_y = 0$ for $\alpha = 90$ deg.

The angular velocity vector Ω now has the following components in the body axes system:

$$p = \Omega \cos\alpha \cos\chi \tag{7.91}$$

$$q = -\Omega \cos\alpha \sin\chi \tag{7.92}$$

$$r = \Omega \sin\alpha \tag{7.93}$$

7.5.1 Balance of Forces in Steady-State Spin

With $\dot{U} = \dot{V} = \dot{W} = 0$, Eqs. (7.74–7.76) reduce to

$$F_x = m(qW - rV) \tag{7.94}$$

$$F_y = m(Ur - pW) \tag{7.95}$$

$$F_z = m(pV - Uq) \tag{7.96}$$

Substituting for U, V, W from Eqs. (7.80–7.82) for p, q, r from Eqs. (7.91–7.93) and ignoring χ ($\cos\chi = 1, \sin\chi = 0$), we get

$$F_x = m\Omega^2 R \sin\alpha \tag{7.97}$$

$$F_y = 0 \tag{7.98}$$

$$F_z = -m\Omega^2 R \cos\alpha \tag{7.99}$$

Ignoring power effects and resolving the aerodynamic and gravity forces acting on the airplane (Fig. 7.12),

$$F_x = L\sin\alpha - D\cos\alpha + W\cos\alpha = m\Omega^2 R\sin\alpha \tag{7.100}$$

$$F_z = -L\cos\alpha - D\sin\alpha + W\sin\alpha = -m\Omega^2 R\cos\alpha \tag{7.101}$$

Multiply Eq. (7.100) by $\cos\alpha$ and Eq. (7.101) by $\sin\alpha$ and add the two equations to obtain

$$D = W \tag{7.102}$$

With this, substitution in either Eq. (7.100) or (7.101) gives

$$L = m\Omega^2 R \tag{7.103}$$

It so happens that we could have arrived at these simple relations directly by looking at Fig. 7.12. However, in this process of deriving these results using equations of motion, we have obtained some understanding of the kinematics of the spinning motion.

With

$$D = \tfrac{1}{2}\rho U_0^2 S C_D \tag{7.104}$$

$$L = \tfrac{1}{2}\rho U_0^2 S C_L \tag{7.105}$$

we get

$$U_0 = \sqrt{\frac{2W}{\rho S C_D}} \tag{7.106}$$

$$R = \left(\frac{1}{2m\Omega^2}\right) \rho U_0^2 S C_L \tag{7.107}$$

From Eqs. (7.67) and (7.68), we have

$$C_L = C_R \cos\alpha \tag{7.108}$$

$$C_D = C_R \sin\alpha \tag{7.109}$$

Suppose we could determine the angle of attack and spin rate from some other criteria, then we could use Eqs. (7.106) and (7.107) to determine the descent velocity and spin radius.

7.5.2 Balance of Moments

For balance of moments, the sum of all the moments must be zero, regardless of the axes system chosen. Suppose we consider the airplane motion with respect to the spin axis; then the centrifugal forces acting on all the components of the airplane acting radially outward from the spin axis do not produce any moment about the spin axis. Therefore, the net aerodynamic moment about the spin axis must also be zero. This means that the resultant aerodynamic force must also pass through the spin axis. In other words, to determine the equilibrium spin modes, we simply have to find the combination of angle of attack, sideslip, and spin rate at which the resultant aerodynamic force passes through the spin axis. However, the scenario is not this simple. Usually, the aerodynamic data does not contain the magnitude, direction, and point of action of the resultant aerodynamic force. Instead, we usually have the aerodynamic data in the form of lift, drag, side force, pitching, rolling, and yawing moment coefficients in the stability axes system. Using this information, we have to compute the balance of pitching, rolling, and yawing moments about the body axes system to determine the equilibrium spin modes.

For steady-state spin, $\dot{p} = \dot{q} = \dot{r} = 0$. With this, moment Eqs. (7.77–7.79) take the following form:

$$L = qr(I_z - I_y) \tag{7.110}$$

$$M = rp(I_x - I_z) \tag{7.111}$$

$$N = pq(I_y - I_x) \tag{7.112}$$

Here, L, M, and N denote the net external rolling, pitching, and yawing moments acting on the airplane during the steady-state spin. Because we have ignored the power effects, the only external moments acting on the airplane are the aerodynamic moments. The right-hand side of Eqs. (7.110–7.112) represent the moments due to inertia cross coupling effects. Substituting for p, q, and r from Eqs. (7.91–7.93)

in Eqs. (7.110–7.112), take the following form:

$$L = -\frac{\Omega^2}{2} \sin 2\alpha \sin \chi (I_z - I_y) \tag{7.113}$$

$$M = \frac{\Omega^2}{2} \sin 2\alpha \cos \chi (I_x - I_z) \tag{7.114}$$

$$N = -\frac{\Omega^2}{2} \cos^2 \alpha \sin 2\chi (I_y - I_x) \tag{7.115}$$

The above Eqs. (7.113–7.115) can be written as

$$L + L_i = 0 \tag{7.116}$$

$$M + M_i = 0 \tag{7.117}$$

$$N + N_i = 0 \tag{7.118}$$

where L_i is the inertia-rolling moment, M_i is the inertia-pitching moment, and N_i is the inertia-yawing moment as given by

$$L_i = qr(I_y - I_z) \tag{7.119}$$

$$= \frac{\Omega^2}{2} \sin 2\alpha \sin \chi (I_z - I_y) \tag{7.120}$$

$$M_i = rp(I_z - I_x) \tag{7.121}$$

$$= \frac{\Omega^2}{2} \sin 2\alpha \cos \chi (I_z - I_x) \tag{7.122}$$

$$N_i = pq(I_x - I_y) \tag{7.123}$$

$$= \frac{\Omega^2}{2} \cos^2 \alpha \sin 2\chi (I_y - I_x) \tag{7.124}$$

Balance of pitching moments. We have

$$M_i = (I_z - I_x) rp \tag{7.125}$$

$$= \frac{\Omega^2}{2} \sin 2\alpha \cos \chi (I_z - I_x) \tag{7.126}$$

To have a physical understanding of how the inertia-pitching moment arises, let us assume that the masses M_1 and M_2 located at the fuselage extremities represent inertia in yaw I_z and masses M_3 and M_4 located at the wingtips represent the inertia in roll I_x as shown in Fig. 7.17. In a right spin, the inertia-induced pitching couple due to M_1 and M_2 is nose up so as to flatten the spin attitude, whereas that due to M_3 and M_4 is nose down so as to steepen the spin attitude. The net inertial pitching couple is the difference between these two opposing contributions.

An alternative way of understanding the inertia-induced pitching moment is to use the gyroscopic analogy. Let us imagine that the inertias in pitch, roll, and yaw are represented by three gyroscopes located at the airplane's center of gravity as shown in Fig. 7.18. The gyroscope with inertia I_x is aligned along the x-body axis and is assumed to be rotating with an angular velocity p. Similarly, the other two

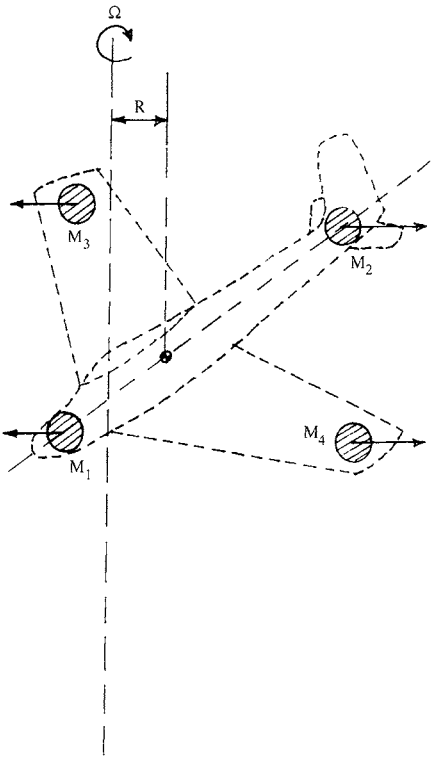

Fig. 7.17 Schematic illustration of inertia-pitching moment.

gyroscopes with I_y and I_z are aligned along y- and z-body axes and are assumed to be rotating with angular velocities of q and r, respectively.

Now if the gyroscope in Fig. 7.18c is disturbed because of an external torque that imparts it a rolling velocity p, then, according to the gyroscopic principles, it will precess in a direction perpendicular to a plane containing both the vectors r and p. Hence, in this case, the angular velocity vector of precession will be along positive y-axis (Fig. 7.19), which corresponds to a noseup pitching motion. Similarly, if the gyroscope in Fig. 7.18a is disturbed by a torque that imparts it a yawing velocity r, it will pitch in a nosedown direction. Thus, the net gyroscopic action will be the difference between these two induced pitching motions.

Generally, $I_z > I_x$ so that the inertia pitching couple is positive or nose up that tends to flatten the spin attitude. For equilibrium, the aerodynamic pitching moment must be negative or nose down. At angles of attack well above the stall, the nosedown aerodynamic pitching moment mainly comes from the horizontal tail with wing making very little contribution.

Balance of rolling moments. As we have seen earlier, unswept wings have a strong autorotative tendency at stall. As a result, for angles of attack beyond the stalling angle, the aerodynamic rolling moment for airplanes having unswept wings is generally prospin. Another factor that contributes to the development

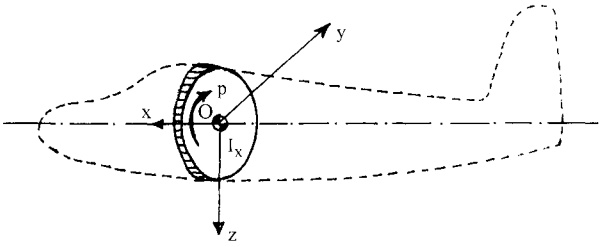

a) Gyroscope aligned along x-axis

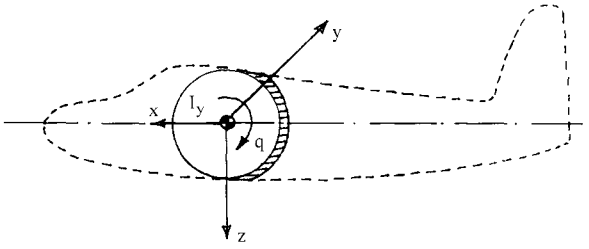

b) Gyroscope aligned along y-axis

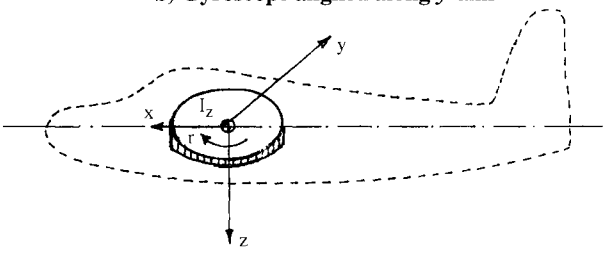

c) Gyroscope aligned along z-axis

Fig. 7.18 Gyroscopic representation of a spinning airplane.

of aerodynamic rolling moment is the dihedral effect $C_{l\beta}$. However, beyond the stalling angle, the magnitude of $C_{l\beta}$ is quite small. Therefore, for airplanes with unswept wings, a major contribution to rolling moment comes from the wings, which produce autorotative or prospin rolling moments for $\alpha \geq \alpha_{\text{stall}}$. Therefore, for such airplanes the inertia-rolling moment must be antispin to achieve the required balance of rolling moments. The inertia-rolling moment is given by

$$L_i = (I_y - I_z)qr \tag{7.127}$$

$$= \left(\frac{\Omega^2}{2}\right) \sin 2\alpha \sin \chi (I_z - I_y) \tag{7.128}$$

Thus, if $\chi = 0$, the inertial-rolling moment is zero. Because the wing tilt directly depends on the angle χ, we observe that a wing tilt one way or the other is necessary to achieve the rolling-moment balance.

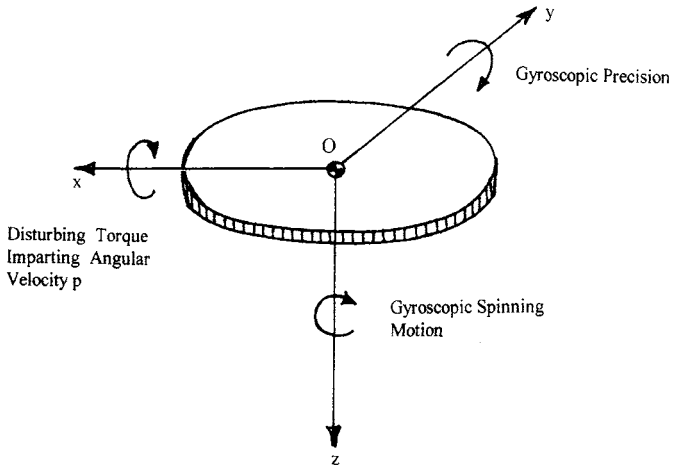

Fig. 7.19 Schematic illustration of gyroscopic precision.

A physical explanation using the lumped wing or fuselage masses is difficult in this case. The gyroscopic analogy comes in handy. If the gyroscope in Fig. 7.18b with moment of inertia I_y and rotating about the y-axis with an angular velocity q is disturbed with yaw rate r, it will roll to the right. Similarly, the gyroscope in Fig. 7.18c with moment of inertia I_z aligned along the z-body axis and rotating with an angular velocity r disturbed by a pitching velocity q will roll to the left. The net rolling motion will be the difference between the two induced motions. Usually, $I_z > I_y$ so that the inertia-induced rolling moment is negative or antispin.

Balance of yawing moments. We have

$$N_i = (I_x - I_y)pq \tag{7.129}$$

$$= \left(\frac{\Omega^2}{2}\right)\cos^2\alpha \sin 2\chi (I_y - I_x) \tag{7.130}$$

As in the case of balance of rolling moments, we observe that the wing tilt plays an important role in the balance of yawing moments.

The concept of lumped fuselage and wing masses can be used to understand the inertia yawing moment as shown in Fig. 7.20 for an aircraft in positive or right spin. In Fig. 7.20a, the wing tilt is negative (right wing above the horizontal, $\theta_y < 0$, $\chi > 0$), and we observe that the fuselage masses M_1 and M_2 representing inertia in pitch I_y produce a prospin yawing moment and the wing masses M_3 and M_4 representing inertia in roll I_x produce an antispin yawing moment. The net inertia-induced yawing moment is the difference of these two contributions. If $I_y > I_x$, then the fuselage masses dominate and the induced yawing moment is prospin. On the other hand, if $I_x > I_y$, the wing masses will dominate and the inertia-yawing couple will be antispin.

If the wing tilt is the other way, i.e., $\theta_y > 0$ or $\chi < 0$ as shown in Fig. 7.20b, then the nature of each contribution changes. The wing masses M_3 and M_4 produce

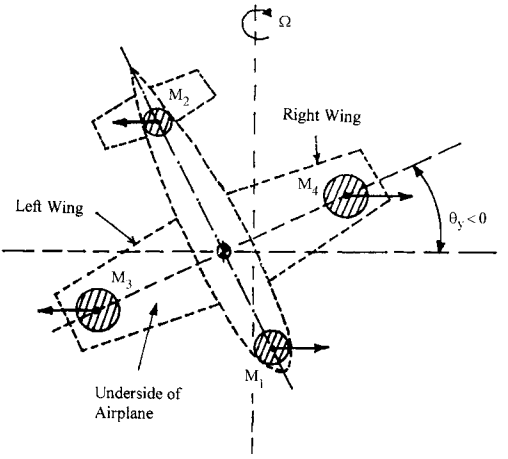

a) Negative wing tilt, $\theta_y < 0, \psi > 0$

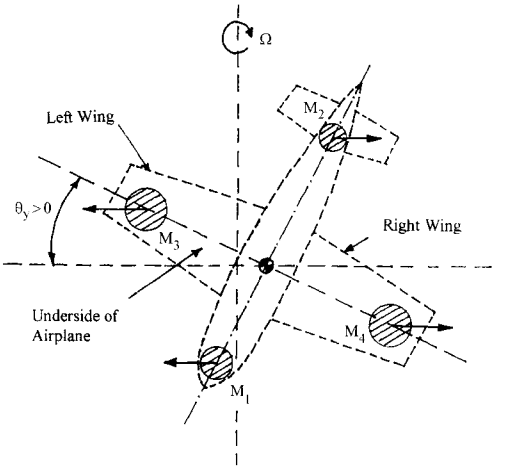

b) Positive wing tilt, $\theta_y > 0, \psi < 0$

Fig. 7.20 Schematic illustration of inertia-yawing moment in spin.

prospin yawing moment, whereas fuselage masses produce antispin yawing moment. If $I_y > I_x$, then the inertia yawing couple will be antispin and, if $I_x > I_y$, it will be prospin.

This simple concept of lumped masses helps us understand how important the wing tilt is in the establishment of equilibrium spin modes. Generally, in a right spin, the majority of the airplanes have a small positive wing tilt ($\theta_y > 0$, $\chi < 0$) and a small outward sideslip (sideslip to port wing, $\beta < 0$).

The contribution to aerodynamic yawing moment mainly comes from the fuselage and vertical tail. The cross-sectional shape of the fuselage has a strong influence on the fuselage contribution.[18,19] In particular, the aft cross sections have a stronger influence owing to their large moment arm with respect to the center of gravity. The cross sections with flat-bottom surfaces contribute to prospin yawing moment, whereas those with rounded-bottom surfaces generate antispin yawing moments.

The effectiveness of the vertical tail and the rudder in spin depend on the extent of shielding of these components due to the wake of the horizontal tail as shown in Fig. 7.21. A deflection of the elevator also has an effect on the shielding of the vertical tail and rudder surfaces. A downward deflection of the elevator increases the shielded area, whereas an upward deflection alleviates the shielding effect.

The nature and extent of shielding of the vertical tail and rudder surfaces also depend on the relative placement of the horizontal tail with respect to the vertical tail as shown in Fig. 7.22. In Fig. 7.22a the aft-body part A and the part B of the body below the horizontal tail contribute to the yawing moment developed by the fuselage. The unshielded part C of the rudder contributes to the rudder effectiveness in generating yawing moments. We observe that the tail design of Fig. 7.22a results in substantial shielding of the rudder. By moving the horizontal tail further aft as in Fig. 7.22b, the shielding of the vertical tail and the rudder

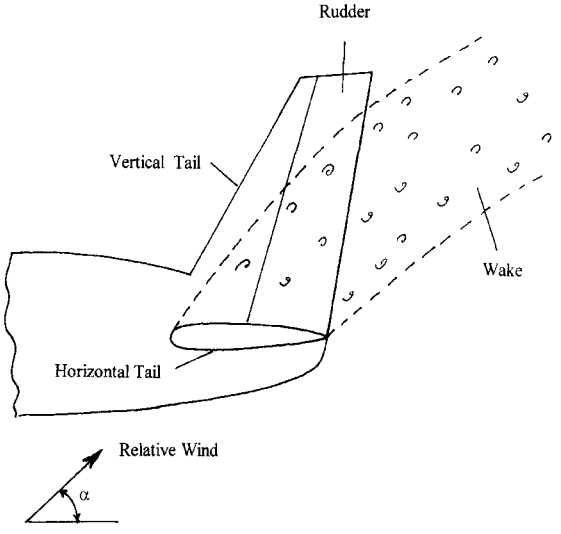

Fig. 7.21 Schematic illustration of shielding effect on vertical tail and rudder.

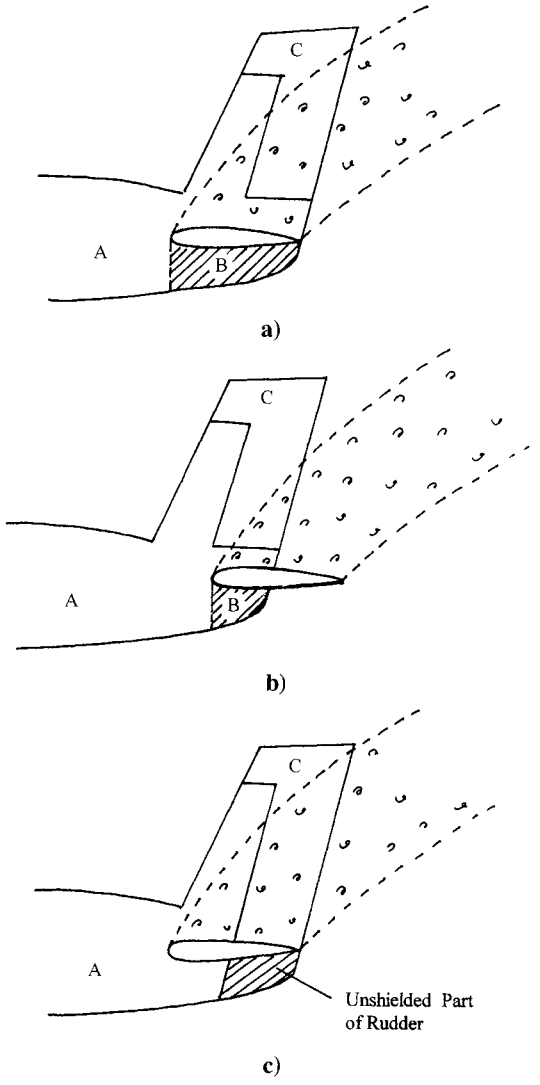

Fig. 7.22 Effect of vertical tail design on shielding effect.

can be reduced. Also, extending the rudder below the horizontal tail as shown in Fig. 7.22c improves rudder effectiveness.

7.6 Spin Recovery

The FAR Part 23[20] requires that, for a normal recovery, a single-engine airplane be capable of recovering from one-turn spin or from a 3-s spin, whichever takes longer, in no more than an additional turn using normal recovery controls.

The standard method of spin recovery as given in so-called "NACA Recovery Procedure" for conventional single-engine light airplanes[21,22] is as follows: move the rudder briskly against the spin, followed by forward stick about one-half turn later while maintaining neutral ailerons. It has been found that this recovery technique is effective in majority of the test cases NASA has evaluated over the years on a variety of single-engine light general aviation airplanes.[11]

The role of ailerons as recovery controls depends on the mass and inertia distribution of the airplane. For an airplane that has most of its mass concentrated into a long fuselage and has relatively lighter wings with a short span ($I_y/I_x > 1$), then the aileron applied in the direction of the spin (or direction of rolling) tends to assist the recovery. The longer the fuselage and greater the weight concentrated in nose and tail, the larger will be the numerical value of the ratio I_y/I_x and greater will be the effect of in-spin ailerons in aiding the recovery. For an airplane that has heavy wings and a large wing span giving $I_y/I_x < 1$, then out-spin ailerons or ailerons applied against the direction of spin (or the direction of roll) is most beneficial. Such a situation exists for airplanes fitted with wing tip tanks. Once again, the smaller the numerical value of the ratio I_y/I_x, the greater will be the effect of out-spin ailerons in aiding the recovery process.

Application of the opposite rudder slows down the spin rate and steepens the spin attitude. While the spin rate is decreasing because of the opposite rudder, the elevator becomes increasingly effective in assisting the recovery. However, an opposite sequence of operation, i.e., one in which the elevator movement preceeds the rudder movement, is decidedly objectionable and may result in an aggravated spin, often resulting in higher rate of rotation and, for some configurations, it may even result in the development of flat spin.

For some airplanes, it may be difficult to recover from a flat spin using normal recovery techniques. Such airplanes often make use of a spin-chute to effect a recovery from flat spin (Fig. 7.23). The opening of the spin-chute generates a nose-down pitching moment in addition to slowing the yaw rate. When the yaw rate decreases, application of forward stick (elevator up) results in a successful recovery.

A typical time history of a spin entry, developed spin, and recovery is shown in Fig. 7.24.[23] The prospin controls for this aircraft consist of full-aft stick, full-rudder deflection in the direction of spin, and full-aileron deflection against the spin. As shown in Fig. 7.24, full-aft stick is gradually applied from 10 to 17 s. At about 17 s, full right rudder ($\delta_r < 0$) for right spin and antispin aileron ($\delta_a > 0$, right aileron to roll to left) are applied. For the next 5–6 s, the angle of attack and yaw rate build up. Around 25 s, the airplane has entered into a right spin, but it takes about two turns to establish a steady-state spin as indicated by a steady value of angle of attack around 52 to 55 deg and a steady value of yaw rate around 110 deg/s. After six complete turns, recovery controls (opposite rudder, stick forward, and ailerons neutral) are

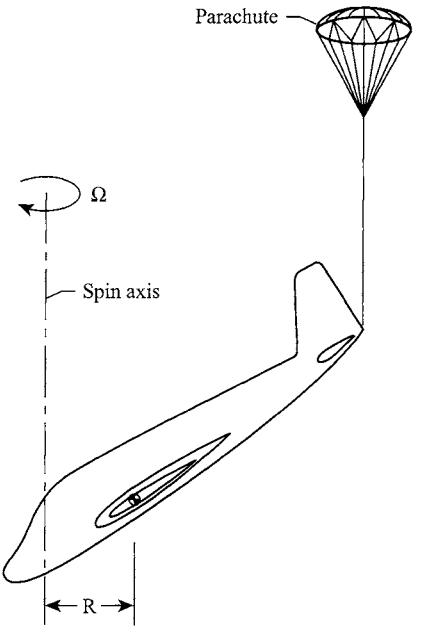

Fig. 7.23 Parachute deployment for spin recovery.

applied. The aircraft recovers successfully and returns to normal steady-level flight within next 5–10 s.

7.7 Geometrical Modifications to Improve Spin Resistance

7.7.1 Modification to Wing

The autorotational characteristics of the wing have a large impact on the stall–spin behavior of the airplane. Eliminating or reducing the autorotative tendency of the wings can greatly improve the spin resistance of the airplane.

One modification to the wing that has been successfully tested by NASA on a number of general aviation airplanes is the reshaping of the wing leading edge of the outer wing panels. The modification consists of a chord extension of about 3%, a drooped-nose airfoil design, and an abrupt discontinuity between the undrooped inner wing and drooped outer wing.[23–25] An application of this method to a general aviation airplane is shown in Fig. 7.25. The basic airplane (Fig. 7.25a) had an untwisted wing with a NACA 64_2415 airfoil section. The modification extended from 57–95% semispan locations as shown in Fig. 7.25b. The variation of the resultant force coefficient of the basic airplane and that with the modification are shown in Fig. 7.25c. We observe that the basic airplane exhibits the usual drop in the resultant force coefficient at stall (around $\alpha = 20$ deg) that leads to instability

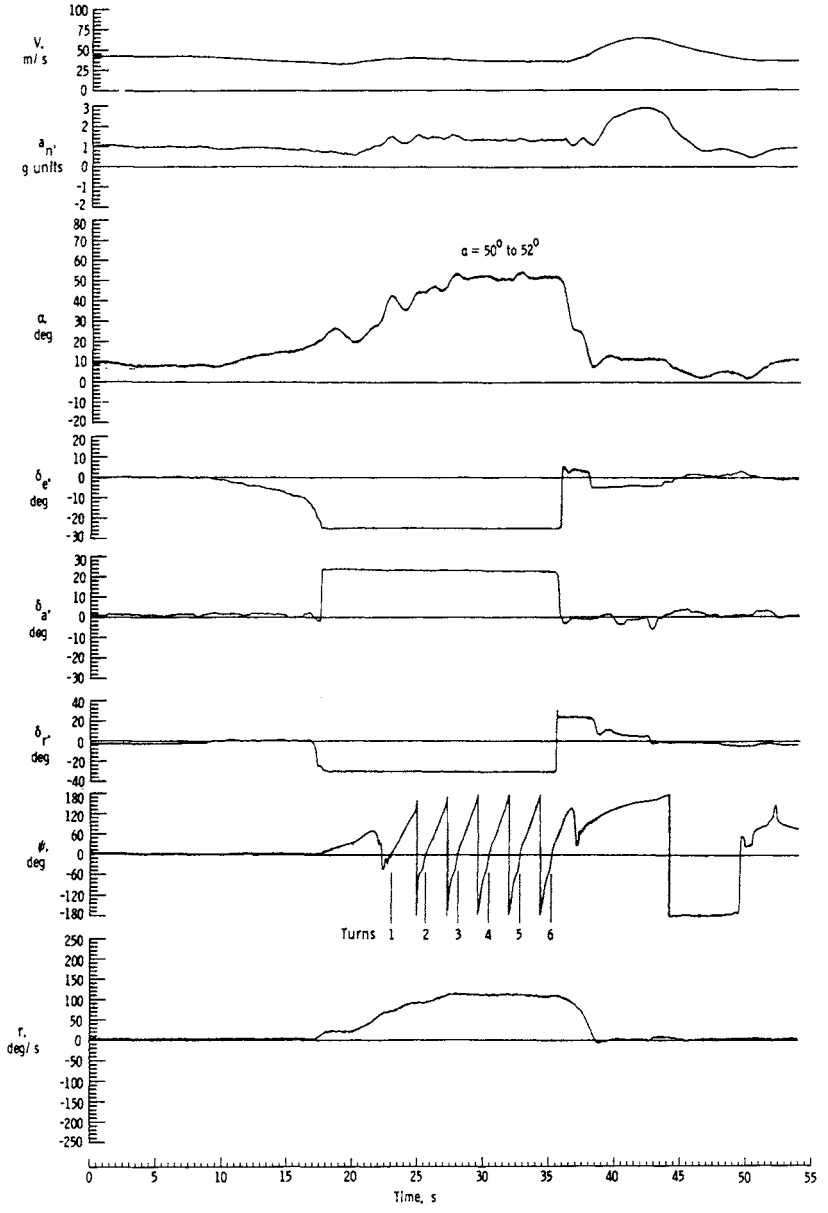

Fig. 7.24 Time history of a spinning airplane.[23]

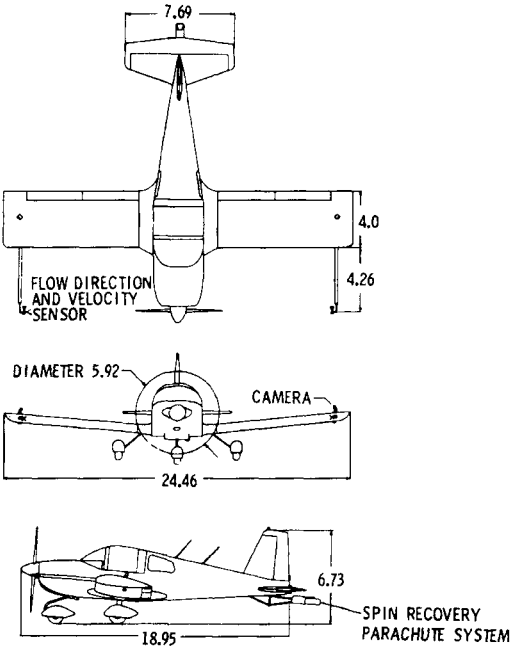

Test airplane A (Dimensions given in feet).

a)

Fig. 7.25 An example of wing leading-edge modification.[23,24]

in roll and autorotation, whereas the modified configuration does not exhibit such tendency for the range of angle of attack shown in Fig. 7.25c.

The basic aircraft exhibited two spin modes, one at $\alpha = 46$ deg and another at $\alpha = 61$ deg. However, the modified airplane was highly resistant to enter the spin.[25]

The aerodynamic phenomenon responsible for this beneficial effect is a strong vortex-type flow that originates at the leading edge discontinuity and tails over the upper surface of the wing functioning like an aerodynamic fence that prevents the spreading of the stalled inboard flow towards the wingtips. As a result, the drooped outboard wing panels remain effective and generate lift to very high angles of attack.[11]

7.7.2 Fuselage Modifications

The aft sections of the fuselage have a relatively stronger influence on the autorotational/spin behavior of the airplane. Hence, modifications to aft fuselage sections will be more effective in controlling the spin behavior. Examples of such modifications tested by NASA[19] include rounding of the bottom surface of the aft fuselage and installation of strakes on the underside of the aft fuselage as schematically depicted in Fig. 7.26. Modifications similar to those shown in Fig. 7.26 result

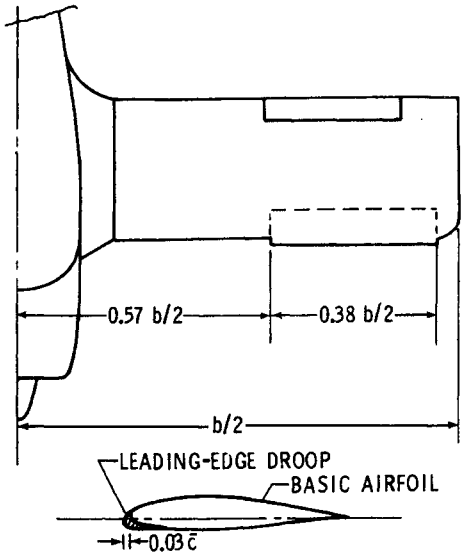

Wing leading-edge modification to outboard wing panel of airplane A.

b)

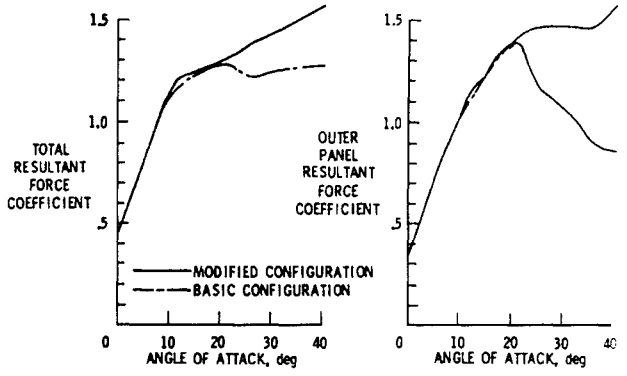

c)

Fig. 7.25 An example of wing leading-edge modification,[23,24] continued.

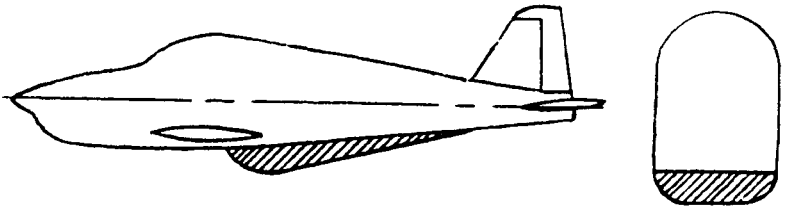

a) Rounded bottom

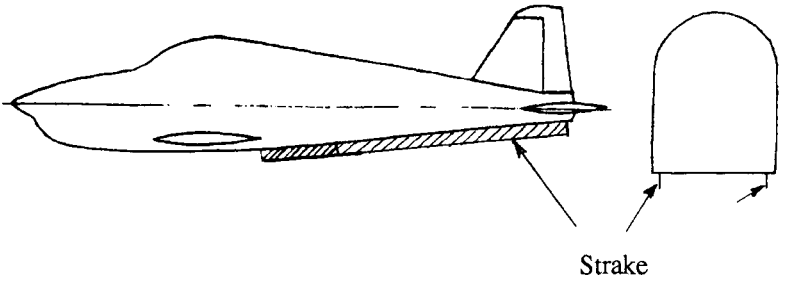

b) Strakes

Fig. 7.26 Examples of modification of fuselage geometry.

in significant improvement in spin resistance of light general aviation airplanes. The spins exhibited by modified airplanes are much steeper and slower compared to the baseline airplanes.[19]

The aerodynamic flow mechanisms giving rise to these beneficial effects are discussed elsewhere.[26,27] Essentially, these modifications alter the sectional side force coefficient characteristics from prospin type A to antispin type B (see Fig. 7.8). As a result, the fuselage contribution becomes more damping in nature.

Example 7.2

A light single-engine, general aviation airplane has the following data: gross weight = 10,915 N, wing span = 9.9822 m, wing area = 13.53 m^2, mean aerodynamic chord = 1.34 m, $I_x = 2304\ kg/m^2$, $I_y = 2602\ kg/m^2$, and $I_z = 4336\ kg/m^2$.

This aircraft has a steady spin mode at an angle of attack of 40 deg. The aircraft takes about 3 min per turn and spins with right wing 5 deg below the horizontal plane. Assuming that the resultant force coefficient at 40 deg angle of attack is equal to 1.2, determine 1) velocity of descent, 2) spin radius as a fraction of wing semispan, 3) angular velocity components in the body axes system, and 4) aerodynamic moments acting on the airplane during the steady-state spin. Assume sea level conditions.

Solution. We have

$$\sin\theta_y = -\cos\alpha \sin\chi$$

With $\theta_y = 5$ deg and $\alpha = 40$ deg, we get $\chi = -6.5326$ deg.

The angular velocity components are given by

$$p = \Omega \cos\alpha \cos\chi$$

$$q = -\Omega \cos\alpha \sin\chi$$

$$r = \Omega \sin\alpha$$

We have

$$\Omega = \frac{360}{3}$$

$$= 120 \text{ deg/s}$$

$$= 2.0942 \text{ rad/s}$$

Substituting, we get

$$p = 91.3285 \text{ deg/s}$$

$$q = 10.4578 \text{ deg/s}$$

$$r = 77.1298 \text{ deg/s}$$

We have $C_R = 1.2$. The lift and drag coefficients are given by

$$C_L = C_R \cos\alpha$$

$$C_D = C_R \sin\alpha$$

Substituting, we get $C_L = 0.9193$ and $C_D = 0.7713$.

We have $W = 10{,}915$ N, $\rho = 1.225$ kg/m^3, and $S = 13.53$ m^2. The velocity of descent is given by

$$U_0 = \sqrt{\frac{2W}{\rho S C_D}}$$

Substituting, we get $U_0 = 41.3236$ m/s. The spin radius is given by

$$R = \left(\frac{1}{2m\Omega^2}\right) \rho U_0^2 S C_L$$

where $m = W/g$. Substitution gives $R = 2.6664$ m or, in terms of wing semispan,

$$\frac{2R}{b} = \frac{2 \times 2.6664}{9.9822}$$

$$= 0.5342$$

Thus, we see that the spin radius is close to one-half of wing semispan.

The inertia moments are given by

$$M_i = rp(I_z - I_x)$$

$$L_i = qr(I_y - I_z)$$

$$N_i = pq(I_x - I_y)$$

In the above equations, the values of p, q, and r are in rad/s. Substitution gives

$$M_i = 4359.5633 \text{ Nm}$$

$$L_i = -425.9929 \text{ Nm}$$

$$N_i = -86.6869 \text{ Nm}$$

For steady-state spin, the sum of aerodynamic and inertial moments is zero. Therefore,

$$M_{\text{aero}} = -4359.5633 \text{ Nm}$$

$$L_{\text{aero}} = 425.9929 \text{ Nm}$$

$$N_{\text{aero}} = 86.6869 \text{ Nm}$$

Converting to coefficient form, we get

$$C_{m,\text{aero}} = \frac{M_{\text{aero}}}{q S \bar{c}} = -0.2299$$

$$C_{l,\text{aero}} = \frac{L_{\text{aero}}}{q S b} = 0.003$$

$$C_{n,\text{aero}} = \frac{N_{\text{aero}}}{q S b} = 0.0006$$

7.8 Summary

In this chapter, we have discussed two classes of flight where the longitudinal and lateral-directional motions of the airplane are strongly coupled. The first case was the inertia coupling or roll coupling problem where a steadily rolling aircraft experiences instability as the roll rate is increased. We observed that an aircraft having a higher level of directional (yaw) stability compared to longitudinal (pitch) stability experiences a divergence in pitch, whereas an aircraft deficient in directional stability is susceptible to a yaw divergence. The roll rates at which an aircraft experiences either of these two instabilities depend on its inertia characterisitics. As the roll rate is further increased, the aircraft becomes stable again, but this time it is spin stabilized about its longitudinal body axis.

The other class of problems we considered is the airplane spin. The autorotational tendency of the unswept wings at stall is the driving mechanism for light general aviation airplanes to enter into a spin. Whether the steady-state spin is established or not depends on the balance between the aerodynamic and inertia moments. If such a balance is not achieved, the spin remains oscillatory. The wing tilt plays an important role in the establishment of a steady-state spin. The magnitude and sign of the inertia-rolling and yawing moments depend on the wing tilt.

Also, the wing tilt affects the sideslip, thereby affecting the aerodynamic rolling and yawing moments. The application of opposite rudder followed by a forward stick is the standard recovery procedure for most of the light general aviation airplanes. However, the use of ailerons for recovery depends on the mass and inertia characteristics of the airplane. On some airplanes, prospin ailerons assist recovery, whereas on others it may be the opposite. Modifying the outboard leading edge of the wing considerably helps improve the spin resistance. Also, some modifications to aft fuselage geometry such as rounding the bottom surface or installing strakes increases the damping effect of the fuselage in spin.

References

[1]Philips, W. H., "Effect of Steady Rolling on Longitudinal and Lateral Stability," NACA TN 1627, June 1948.

[2]Pinsker, W. J. G., "The Theory and Practice of Inertia Coupling," *Journal of the Royal Aeronautical Society*, Vol. 73, Aug. 1973, pp. 695–702.

[3]Gates, O. B., Jr., and Woodling, C. H., "A Theoretical Analysis of the Effects of Engine Angular Momentum on Longitudinal and Directional Stability in Steady Rolling Maneuvers," NACA TN 4249, April 1958.

[4]Hacker, T., and Oprisiu, C., "A Discussion on the Roll Coupling Problem," *Progress in Aerospace Sciences*, Vol. 15, 1974, pp. 151–180.

[5]Schy, A. A., and Hannah, M. E., "Prediction of Jump Phenomena in Roll-Coupled Maneuvers of Airplanes," *Journal of Aircraft*, Vol. 14, No. 4, April 1977, pp. 375–382.

[6]Sternfield, L., "A Simplified Method for Approximating the Transient Motion in Angles of Attack and Sideslip During Constant Rolling Maneuver," NACA Rept. 1344, 1958.

[7]Blakelock, J. H., *Automatic Control of Aircraft and Missiles*, Wiley, New York, 1965.

[8]Knight, M., "Wind Tunnel Tests on the Autorotation and the Flat Spin," NACA Rept. 273, 1927.

[9]Polhamus, E. C., "Effect of Flow Incidence and Reynolds Number on Low Speed Aerodynamic Characteristics of Several Noncircular Cylinders with Application to Directional Stability and Spinning," NASA TR R-29, 1959.

[10]Anderson, S. B., "Historical Overview of Stall/Spin Characteristics of General Aviation Aircraft," AIAA Paper 78-1551, Aug. 1978.

[11]Chambers, J. R., and Paul Stough, H., III., "Summary of NASA Stall/Spin Research for General Aviation Configurations," AIAA Paper 86-2597, 1986.

[12]DiCarlo, D. J., Stough, H. P., III., Glover, K. E., Brown, P. W., and Patton, J. M., Jr., "Development of Spin Resistance Criteria for General Aviation Airplanes," AIAA Paper 86-9812, 1986.

[13]Gates, S. B., and Bryant, L. W., "The Spinning of Aeroplanes," ARC R and M No. 1001, 1926.

[14]Pamadi, B. N., and Taylor, L. W., Jr., "A Semi-Empirical Method for Estimation of Aerodynamic Characteristics of Steadily Spinning Light Airplanes," NASA TM 4009, Dec. 1987.

[15]Pamadi, B. N., and Taylor, L. W., Jr., "Estimation of Aerodynamic Characteristics of Steadily Spinning Light Airplanes," *Journal of Aircraft*, Vol. 21, No. 12, 1984, pp. 943–954.

[16]Adams, W. M., Jr., "Analytical Prediction of Airplane Equilibrium Spin Characteristics," NASA TN D-6926, Nov. 1972.

[17]Dickinson, B., *Aircraft Stability and Control for Pilots and Engineers*, Sir Isaac Pitman and Sons, London, 1968.

[18]Beaurain, L., "General Study of Light Airplane Spin, Aft Geometry, Part I," NASA TTF-17446, June 1977.

[19]Burk, S. M., Bowman, J. S., and White, W. L., "Spin-Tunnel Investigation of the Spinning Characteristics of Typical Single-Engine General Aviation Airplane Designs, I-Low Wing Model A, Effect of Tail Configurations," NASA TP 1009, 1977.

[20]*Airworthiness Standards*, "Normal, Utility and Acrobatic Category Airplanes," *Federal Aviation Regulations*, Vol. III, Part 23, FAA, June 1974.

[21]Neihouse, A. I., and Klinar, W. J., "Status of Spin Research for Recent Airplane Designs," NASA TR R-57, 1960 (Supersedes NACA RM L57F12).

[22]Bowman, J. S., "Summary of Spin Technology as Related to Light General Aviation Airplanes," NASA TND-7575, Dec. 1971.

[23]Staff of Langley Research Center, "Exploratory Study of the Effects of Wing-Leading Edge Modifications on the Stall/Spin Behavior of a Light General Aviation Airplane," NASA TP 2011, June 1982.

[24]DiCarlo, D. J., Glover, K. E., Stewart, E. C., and Stough, H. P., "Discontinuous Wing Leading Edge to Enhance Spin Resistance," *Journal of Aircraft*, Vol. 22, No. 4, 1985, pp. 283–288.

[25]Stough, H. P., III., Jordan, F. L., Jr., DiCarlo, D. J., and Glover, K. E., "Leading-Edge Design for Improved Spin Resistance of Wings Incorporating Conventional and Advanced Airfoils," Society of Automotive Engineers, SAE Aerospace Technology Conference and Exposition, Paper 830720, Long Beach, CA, Oct. 14–17, 1985.

[26]Pamadi, B. N., and Pordal, H. S., "Effect of Strakes on the Autorotational Characteristics of Noncircular Cylinders," *Journal of Aircraft*, Vol. 24, No. 2, 1987, pp. 84–97.

[27]Pamadi, B. N., Jambunathan, V., and Rahman, A., "Control of Autorotational Characteristics of Light-Airplane Fuselages," *Journal of Aircraft*, Vol. 25, No. 8, 1988, pp. 695–701.

Problems

7.1 If the aircraft in Example 7.1 is flying at 175 m/s at an altitude of 8000 m, determine the range of roll rates for divergence in yaw or pitch. Assume $C_{n\beta} = 0.045$ per radian. Except for this change, all the other parameters remain the same.

7.2 The aircraft of solved Example 7.2 has another steady-state spin mode at $\alpha = 55$ deg and takes 2.2 s per turn. Assuming that the aircraft spins with its right wing 3.5 deg below the horizontal plane, determine (a) descent velocity, (b) spin radius in terms of wing semispan, (c) angular velocity components in body-fixed axes system, and (d) inertia and aerodynamic coefficients acting on the airplane.

Assume that the aircraft is operating at an altitude of 6000 m and the resultant force coefficient at $\alpha = 55$ deg is 1.30.